

Copyright
by
Lukas Gerhard Georg Gradl
2017

The Thesis Committee for Lukas Gerhard Georg Gradl
certifies that this is the approved version of the following thesis:

**A "Heat Pipe"-style Recirculating Lithium Oven for
Entrainment into Supersonic Helium Beams**

COMMITTEE:

Mark G. Raizen, Supervisor

Greg O. Sitz

**A "Heat Pipe"-style Recirculating Lithium Oven for
Entrainment into Supersonic Helium Beams**

by

Lukas Gerhard Georg Gradl

THESIS

Presented to the Faculty of the Graduate School of

The University of Texas at Austin

in Partial Fulfillment

of the Requirements

for the Degree of

MASTER OF ARTS

THE UNIVERSITY OF TEXAS AT AUSTIN

December 2017

Acknowledgments

First of all, I would like to thank my advisor Mark Raizen. Mark is a great physicist, whose amazing ideas, insights, and intuition continuously inspire me. But beyond that, I want to thank Mark for the friendly and supportive atmosphere he fosters in his group that I had the pleasure of joining in September of 2015. At that point I had just finished my undergraduate program and came here to Austin on the Würzburg exchange program funded by the German Academic Exchange Service (DAAD), both of which I gratefully acknowledge. As my plans changed to extend my stay beyond the originally envisioned time frame, Mark went to great lengths to help me in my endeavor. I am very thankful for his immense support during this time and his continued support to this day. It is an honor and a pleasure to be a member of his group.

When I joined the group, I knew nothing about doing experiments. I owe all my experimental expertise to the two people who were always there to steer me in the right direction and keep me from making horrible mistakes or helped me clean up after those. I remember certain vacuum systems and certain nozzles that I would have completely ruined without their intervention. And all those countless solder joints and all those countless boards that would have broken off immediately had they not shown me how to solder. My limited attempts at machining, optics and lasers, electrical fabrication, pumps,

experimental care. Without your help I would have never succeeded with this work, so I owe a big thank you to Kevin Melin and Yu Lu. It has been a pleasure working with you and I will miss the hours that we spent together in the lab.

For his efforts on my early integration into the group I would like to thank Jianyong Mo. I would like to thank Karl Burkhardt for valuable insights into heat pipe ovens and the English language. I would like to thank Pavel Nagornykh for his work on the heat pipe before I joined that effort and his guidance and mentorship during my work on this problem. I would also like to thank Harry Ha, Logan Hillberry, Yi Xu, and Jordan Zesch for their work on the slower project and for the pleasant time that we spent together. I would like to thank Georgios Stratis for the many interesting discussions we had. I would like to also thank Akarsh Simha for his inspiration and his advice. I would like to thank Igal Bucay, Erik Anciaux, Jamie Gardner, and Ahmed Helal for their input, help, and support. Thank you all, friends!

I would also like to thank Olga Vera, Matt Ervin, and John Keto for their help in navigating the administrative difficulties of graduate school.

A "Heat Pipe"-style Recirculating Lithium Oven for Entrainment into Supersonic Helium Beams

Lukas Gerhard Georg Gradl, M.A.
The University of Texas at Austin, 2017

Supervisor: Mark G. Raizen

This thesis presents the work on a new oven design optimized for the entrainment of lithium into a pulsed supersonic beam of helium. The proposed oven does not pollute the vacuum with lithium atoms that are not entrained, but instead is designed to capture and recirculate all atoms that are not carried away by the supersonic beam. The transportation of lithium inside the oven is reminiscent of a heat pipe, coining the nickname of the oven: Lithium is evaporated in a hot reservoir, recondensed at a cold surface, and recirculated to the hot reservoir using capillary action.

The supersonic helium beam is generated by an Even-Lavie valve yielding a cold and collimated flow of gas. The supersonic beam can be further collimated by using a skimmer. Two different heat-pipe oven designs are investigated in this thesis, one for entrainment downstream of the skimmer and one for entrainment upstream of the skimmer.

Downstream of the skimmer, the lithium that is carried in the helium beam behind the oven is much hotter and slower than the carrier gas. This is due to the low density of the helium beam past the skimmer, which does not support enough collisions with the lithium atoms to reach equilibrium.

Upstream of the skimmer, the helium density is higher and the beam behaves in part like continuous flow and the interaction with the oven heats the supersonic beam considerably. The lithium content in the beam that was measured past the skimmer is faster and hotter than the helium flow. It is also not properly entrained, but pushed along by the helium beam.

From these experiments it is obvious, that entrainment depends crucially of the local properties of the supersonic beam at the entrainment site. To be more flexible in the choice of this parameter, a new design for a heat-pipe oven is proposed, which allows for linear translation along the propagation direction of the beam, upstream of the skimmer.

Table of Contents

Acknowledgments	iv
Abstract	vi
List of Figures	x
Chapter 1. Introduction	1
Chapter 2. Supersonic Beams	4
2.1 Overview	4
2.2 Beam Simulation using Direct Simulation Monte Carlo (DSMC)	11
Chapter 3. Methods for Entraining Lithium and the Idea of the Recirculating Oven	18
3.1 Effusive Oven	18
3.2 Directional Oven	20
3.3 Flashed Ribbons	22
3.4 Recirculating Oven: The Heat Pipe	24
Chapter 4. Measurement Techniques	28
4.1 Residual Gas Analyzer	28
4.2 Langmuir-Taylor Detector	30
4.3 Optical Resonant Absorption	32
4.3.1 Overview	32
4.3.2 Saturated Absorption Spectroscopy	34
Chapter 5. Heat Pipe Entrainment behind the Skimmer	37
5.1 Design of the Heat Pipe	37
5.2 Controlling Hydrogen Desorption	40
5.3 Effects on the Helium Beam and Entrainment	41

Chapter 6. Heat Pipe Entrainment before the Skimmer	49
6.1 Design of a fixed Heat Pipe	49
6.1.1 Beam Head	51
6.1.2 Reservoir	52
6.1.3 Heater Assembly	54
6.1.4 Comparison of Expected Flux to the Capillary Oven . .	56
6.2 Thermal Behavior	57
6.3 Interaction with the Helium Beam and Entrainment	64
Chapter 7. Conclusion	71
Chapter 8. Future Work	73
8.1 Linear Translation along the Beam Path	73
8.2 Active Cooling System	75
References	77
Vita	87

List of Figures

2.1	Conceptual sketch of the functional parts of the Even-Lavie valve. The stainless steel tube (black lines) is sandwiched between the nozzle and the gas supply assembly. The interfaces are sealed with two Kapton gaskets. Inside the tube, the magnetic plunger is held in place by the spring, creating a seal over the aperture in the front gasket. When current is pulsed through the coil, the plunger moves back and gas can flow out of the nozzle. The arrow marks the propagation direction of the gas beam.	5
2.2	Flow-field of the underexpanded flow from a diverging nozzle. As the gas exits the nozzle at pressure p_e , it expands and its Mach number increases. Since information about the background pressure p_0 cannot propagate upstream the supersonic beam, the beam expands until its pressure is smaller than p_0 . At this point, the beam is compressed in a set of oblique shock waves called the barrel shock. This decreases its cross sectional area, reduces its Mach number, and increases the pressure until the original pressure p_e is reached at the Mach disk. The beam is thus again underexpanded and the cycle may repeat.	7
2.3	Flow-field of the underexpanded flow from a diverging nozzle. The figure shows conceptually the location of the quitting surface, the surface that delimits the continuous from the molecular flow regime, and the placement of the skimmer.	8
2.4	Number density in the flow-field in a conical nozzle. The flow is anisotropic, favoring the forward direction along the nozzle axis, as seen from the elongated arcs in the contour lines. . . .	14
2.5	Mach number in the flow-field in a conical nozzle. Inside the nozzle, close to the walls, there are collisions with the walls that slow the beam, however, close to the axis of the nozzle the beam quickly becomes supersonic. Once outside the nozzle, the beam becomes highly supersonic.	15
2.6	Temperature in the flow-field in a conical nozzle. Inside the nozzle, off of the central axis the beam is heated due to collisions with the nozzle walls, however the flow near the center of the nozzle stays cold. After exiting the nozzle the beam expands and cools significantly.	16

3.1	Conceptual drawing of the effusive oven in the supersonic beam line. The oven consists of a heated reservoir containing the lithium payload. The oven is open to vacuum at the top allowing the lithium to escape into the chamber volume and entrain into the supersonic beam.	18
3.2	Vapor pressure of lithium as a function of temperature. The dotted line indicates the melting point of lithium. The vapor pressure increases and surpasses the ambient pressure of 10^{-7} torr (10^{-5} Pa) at about 370 K before it liquefies. The vapor pressure increases further to the order of 1 Pa at 900 K. Data from [37].	19
3.3	Conceptual drawing of the directional oven in the supersonic beam line. The top opening of the oven is filled with an array of micro-capillaries, which only allow lithium atoms to escape if their trajectories are aligned with the axis of the micro-capillary array.	21
3.4	Conceptual drawing of the directional oven loading the ribbon. The ribbon is mounted above the oven so that the supersonic beam passes in between them. The oven constantly deposits lithium on the ribbon, which can be flashed off of the ribbon by pulsing current. This allows us to synchronize the lithium release with the passing of the supersonic beam.	23
3.5	Conceptual drawing of the "heat-pipe" recirculating oven and its position in the path of the supersonic beam: The oven consists of a heated cylindrical reservoir partially filled with liquid lithium (hatched). The lithium that evaporates in the reservoir emerges into the cylindrical beam head, which is aligned with the propagation direction of the supersonic beam. lithium is then either entrained or deposited on the beam head walls, as the geometry is chosen such that there is no direct line of sight from the lithium in the reservoir to the exit holes of the beam head. The lithium on the walls is recirculated into the reservoir through gravity and capillary action.	25
4.1	Illustration of the method of operation of a residual gas analyzer. The heated filament emits electrons that are accelerated towards the anode grid. Neutral atoms that enter the anode grid are bombarded with electrons and ionized. They are then accelerated away from the anode grid and towards the focus plate. After transmission through the hole in the focus plate, the ions enter the quadrupole mass spectrometer.	29

4.2	Schematic of the optical setup for generation of a 670 nm laser tuned to the lithium <i>D2</i> line. The diode laser is locked to a spectroscopy cell using saturated absorption spectroscopy. The frequency reference obtained in this way is then used to lock the tapered amplifier (TA) using a beat-locking technique. The offset acquired in the beat-locking is removed in the two acousto-optical modulators (AOM), which also allow to create two different arbitrary detunings to target different Doppler-shifted velocity groups. $\lambda/2$: half-wave plate, $\lambda/4$: quarter-wave plate, <i>PD</i> : Photodiode.	33
5.1	Conceptual drawing of the heat pipe. It consists of a tube (beam head) that is aligned with the propagation direction of the supersonic beam. The heat pipe is mounted behind the skimmer using the 3.75" CF-flange on both ends. In the middle, the reservoir is attached to the bottom of the beam head. It consists of a cylindrical tube that contains the lithium and can be heated externally.	38
5.2	Drawing of a cross section through the heat pipe along the propagation axis of the supersonic beam. The beam head has thick walls near the center that act as thermal mass to keep the temperature elevated in this region. Close to the flanges, it is thin to minimize heating of attached chambers and, in particular, the skimmer. The reservoir is lined with 160 grooves parallel to its axis. These grooves are 0.015" wide and 0.02" deep and enhance the recirculation of the lithium through capillary action.	39
5.3	Pressure inside the heat pipe at different temperatures. The dots indicate measurements in a heat pipe made from stainless steel 430; diamonds indicate measurements made in a heat pipe consisting of stainless steel 316. The pressure levels in stainless steel 316 rise much higher than in 430 steel. This caused by the liquid lithium, which attacks the 316 steel so that hydrogen absorbed in the volume of the steel can desorbed. For stainless steel 430 the levels are lower since the steel is less corrosive under exposure to liquid lithium.	42

5.4	Transmitted laser power in an absorption measurement as a function of the reservoir temperature. The laser points along the axis of the heat pipe parallel to the propagation direction of the supersonic beam and passes over the opening of the reservoir. As the reservoir temperature increases, the laser power decreases, as the lithium vapor pressure increases and more lithium is emitted from the reservoir. At a temperature of 500 °C and higher, this behavior saturates. This is because at this point, the lithium cloud becomes collisional (diffusive regime) and starts to spread along the axis of the heat pipe. The lithium that spreads out can not be seen with this absorption measurement since it is Doppler-shifted off the laser frequency due to its velocity along the heat pipe axis and along the propagation direction of the laser. As the temperature increases further, the lithium reaches the viewports at the front and back end of the chamber through which the laser passes and starts coating them. This leads to a further decrease in the transmitted power, which does not regenerate when decreasing the temperature. To resume the experiment, the viewports need to be cleaned.	44
5.5	Sample plot showing the signal from the Langmuir Taylor detector measuring lithium and from the RGA measuring helium as a function of arrival time at the Langmuir Taylor detector. The RGA signal has been shifted in time to correct for a 5" difference in path length to the RGA. The supersonic nozzle was opened for 30 μ s at a backing pressure of 304 psi (2.10×10^6 Pa) to create the shown helium beam. The reservoir of the heat pipe was at a temperature of 530 °C. The amplitudes have been scaled to fit on the same axis. The helium beam arrives at the detector significantly earlier and it is much narrower than the lithium beam. This is a sign of failed entrainment, as there are not enough collisions between helium and lithium atoms to achieve equilibrium between the two species.	47
6.1	Schematic drawing of the "heat pipe" recirculation entrainment oven. The left side shows the heat pipe as it is mounted on a 10" conflat flange. On the right, the structure of the heat pipe is labeled as beam head (a), reservoir (b) and heater assembly (c).	49

6.2	Cross section view of the heat pipe beam head along the propagation direction of the supersonic beam. The inlet and outlet openings for the supersonic beam have a diameter of 0.7", which is approximately 3.5 times larger than the diameter of the skimmer (5 mm). The inside surface of the beam head is angled to allow liquid lithium to flow back into the reservoir. The reservoir attaches to the large cutout at the bottom of the beam head, perpendicular to its axis.	51
6.3	Cross-section through the reservoir perpendicular to its cylindrical axis. Visible are the small cylindrical cutouts on the inside wall that wick liquid lithium back into the reservoir through capillary action. All labeled values are in units of inches. . . .	53
6.4	Temperature profile of the heat pipe when reservoir is held at 900 K. This simulation shows how the temperature drops from the bottom of the reservoir to the beam head. For ideal operation, the reservoir should be hot to generate a large vapor pressure of the liquid lithium, whereas the top part of the reservoir and the beam head stay at cooler temperatures of around 500 K to avoid secondary emission of accumulated lithium atoms. The temperature in the top is however still hot enough for the lithium not to solidify so that it can be recirculated into the reservoir.	58
6.5	View of the assembled heat pipe in the vacuum system during baking. The copper heater assembly is heated to 600 °C and visibly glows. The camera is sensitive to the near infrared which is rendered as violet, which is responsible for the coloring of the glowing copper. In the background, the incandescent filament of the residual gas analyzer is visible. The steel-plated wires in the foreground are thermocouples used to measure the temperature at the top of the beam head and at the bottom of the reservoir, below the heater assembly. The bright spot near the lower edge of the flange in the background is a viewport illuminated from behind.	60
6.6	Temperature at the top of the beam head and at the bottom of the reservoir at different applied electrical heating powers. . .	61
6.7	Schematic of the spacial positions of the heat pipe beam head, the supersonic nozzle, and the skimmer, relative to each other. All values are in units of inch.	64
6.8	RGA measurements of the helium beam and the lithium from the experimental pipe after the skimmer.	66

8.1	Conceptual drawing of the heat pipe oven with a translation stage (left: corner view, right: top view). The heat pipe is held at the top by a stainless steel plate that can be mounted to the holding structure with different offsets in steps of 0.5" by moving the hole pattern along one step. There is a copper block on top of the beam head that serves as a heat sink and is fitted with grooves at the top, that house tubing with flowing air or water (tubing not shown) to actively cool the beam head. . . .	74
8.2	Image of the cooling assembly that mounts on top of the beam head. The copper tubing runs across the top of the heat sink four times and it is recessed into grooves for better thermal coupling. The heat sink approximates the shape of the beam head and fits tightly. There is one hole in the side face of the heat sink that allows for mounting of a thermocouple wire to measure the temperature of the top of the beam head, underneath the heat sink.	76

Chapter 1

Introduction

In 1995, a Bose-Einstein condensate in a dilute gas was first observed [1, 2]. A Bose-Einstein condensate (BEC) is a state of matter, in which its constituent bosonic particles are cooled and condensed enough to reach a quantum degenerate state. Today, more than 20 years after this historic achievement, the field of cold atoms remains exciting.

Cold atoms are used to study turbulence in quantum systems [3, 4, 5], to measure the gravitational constant [6], the fine-structure constant [7], and there are proposals to use cold atoms to measure gravity waves [8], to verify the weak-equivalence principle [9], and to measure the neutrino mass [10]. Applications include atom lasers [11] as well as neutral atom imaging [12, 13] for lithography and microscopy.

All these experiments depend on the ability to create a high flux of cold atoms. A common method used to create cold atoms is laser cooling [14]. This method however relies on a two-level cycling transition in the electron energy structure of the atom or molecule, which might be hard to access or not given at all, in which case excessively complex laser setups are required [15, 16].

A different approach that does not have this shortcoming is to use an

atomic beam from a supersonic valve that produces an inherently cold beam. Supersonic valves like these have been used extensively in physical chemistry [17, 18]. The velocity spread in such a beam is very low, corresponding to temperatures of hundreds of Milli-Kelvin or less. These beams can be used as sources of cold atoms in a variety of ways [19, 20], with one of the most promising being the deceleration of the beam to the lab frame using an adiabatic decelerator. This device utilizes the paramagnetism that can be found or easily achieved in most atoms and molecules to trap the beam in a co-moving, decelerating, magnetic trap and gently reduce its velocity without significant heating [21, 22, 23]. From this starting point, other cooling methods like MOP-cooling [24] can be used to achieve quantum degeneracy.

However, not every material can produce an atomic beam in a supersonic valve. A notable example where this is not possible are metals, which are solid at room and cryogenic temperatures. Materials like this can however be injected into a supersonic beam in a process called entrainment [25]. Once inside the supersonic beam, the entrained particles are sympathetically cooled and thus inherit the beneficial properties of the beam [25].

This thesis will present one such way to achieve entrainment of lithium into a supersonic beam of helium. To this end, chapter 2 reviews the basic properties of supersonic beams. Chapter 3 gives an overview of existing methods of entrainment and outlines the idea of the "heat pipe" which this thesis will analyze in greater detail. Experimental techniques are discussed in chapter 4. Chapters 5 and 6 discuss the experiments that have been performed

with the "heat-pipe"-style oven and review the results. Chapter 7 summarizes the work and chapter 8 outlines next steps to achieve entrainment with this method.

Chapter 2

Supersonic Beams

The goal of this work is to outline a novel oven design for entraining into supersonic beams. This chapter introduces supersonic beams, their creation, and their properties.

2.1 Overview

To create a pulsed supersonic beam, we use a conical Evan-Lavie supersonic valve [26, 27]. A sketch of the nozzle design can be seen in figure 2.1. The valve consists of a conical nozzle facing vacuum. The opening angle of our nozzle is 40° and at the wide end of the conical opening, there is a smooth transition to a 90° face, avoiding sharp edges. The smallest diameter of the nozzle is $100\ \mu\text{m}$ at the stagnation point.

The gas supplied to the nozzle is helium. The gas line assembly and the nozzle are separated by a stainless steel tube, which is sealed to the nozzle and the gas line with two compressional Kapton gaskets. The tube contains a spring-loaded, magnetic plunger, which allows for pulsing of the valve. While at rest, the spring pushes the front face of the plunger into the flat back face of the conical nozzle, thus sealing the exit hole and blocking the outwards flow of

gas. To open the valve and allow gas to exit, the plunger can be actuated by pulsing electrical current through the magnetic coil that surrounds the tube containing the plunger. The magnetic force acting on the plunger lifts it off of the back face of the nozzle, thus disrupting the seal and allowing the gas to flow. After the end of the current pulse, the spring will move the plunger back into its position covering the back face of the nozzle and thus reestablishes the seal.

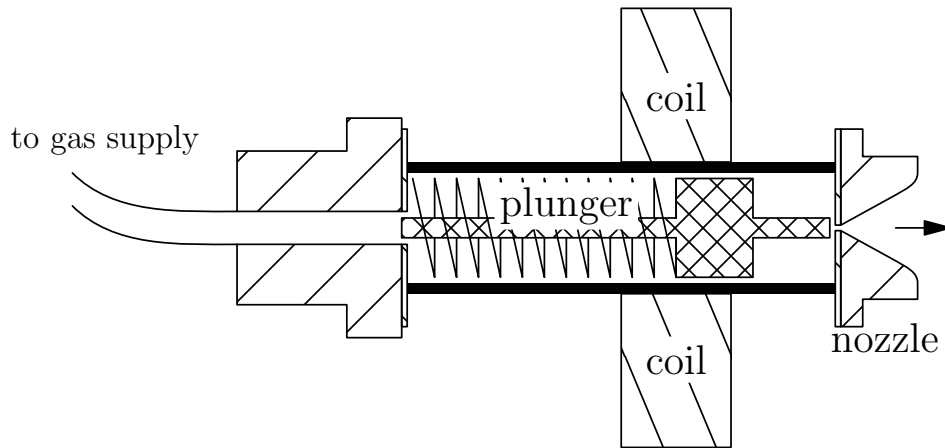


Figure 2.1: Conceptual sketch of the functional parts of the Even-Lavie valve. The stainless steel tube (black lines) is sandwiched between the nozzle and the gas supply assembly. The interfaces are sealed with two Kapton gaskets. Inside the tube, the magnetic plunger is held in place by the spring, creating a seal over the aperture in the front gasket. When current is pulsed through the coil, the plunger moves back and gas can flow out of the nozzle. The arrow marks the propagation direction of the gas beam.

The pressure of the helium in the gas line can be regulated from 100 psi to 700 psi (7×10^5 Pa to 5×10^6 Pa), which corresponds to the stagnation pressure in the nozzle. Upon opening of the supersonic valve, the helium expands

into a vacuum chamber that is kept at pressures on the order of 10^{-7} torr (10^{-5} Pa).

Considering these pressure differences, a steady state flow out of the nozzle can be described as isentropic in regions that do not undergo supersonic shock. This is in particular true for the underexpanded flow from a converging nozzle, which can be a general model for the flow as long as the beam can be described as a continuous medium [28, 29]. A schematic of the flow field that is expected from a steady state flow from a converging nozzle is shown in figure 2.2 [28].

The gas exits the nozzle with a pressure p_e that is much greater than the ambient pressure in the vacuum system p_0 . At the nozzle exit, the beam is already supersonic, with a Mach number $M \gg 1$. The Mach number is defined as the ratio of the beam velocity to the local speed of sound: $M = \frac{v}{c}$, where the sound speed is given by $c = \sqrt{\kappa p / \rho}$, with the pressure p , the density ρ and the ratio $\kappa = c_p / c_V$ of the specific heat at constant pressure c_p and at constant volume c_V . The sound speed c is the speed at which pressure disturbances travel in the medium. If the flow of the beam is supersonic, i. e. at velocities larger than c and thus at Mach numbers larger than 1, then pressure waves can not propagate upstream. This means that the beam travels independently of the flow conditions downstream.

After exiting the nozzle, the flow adapts to the difference between its stagnation pressure and the ambient pressure with an expansion in the radial dimension, perpendicular to its propagation direction and forming fans of ex-

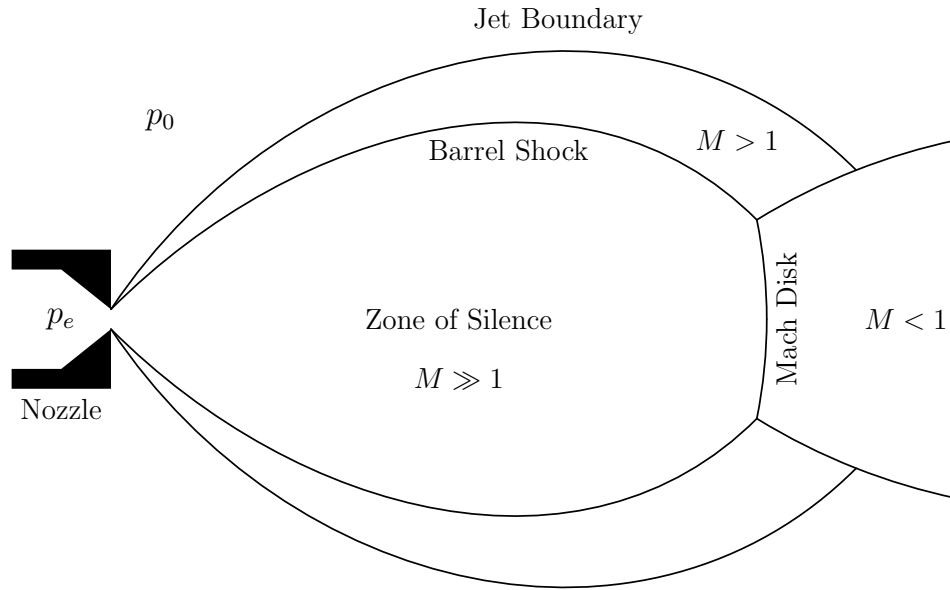


Figure 2.2: Flow-field of the underexpanded flow from a diverging nozzle. As the gas exits the nozzle at pressure p_e , it expands and its Mach number increases. Since information about the background pressure p_0 cannot propagate upstream the supersonic beam, the beam expands until its pressure is smaller than p_0 . At this point, the beam is compressed in a set of oblique shock waves called the barrel shock. This decreases its cross sectional area, reduces its Mach number, and increases the pressure until the original pressure p_e is reached at the Mach disk. The beam is thus again underexpanded and the cycle may repeat.

pansion waves [28]. The jet boundary is thus not cylindrical, but diverging. Along its propagation, the Mach number of the gas beam increases [29]. Since the propagation speed is much greater than the sound speed, the supersonic beam expands further irrespective of the ambient pressure p_0 . This region of the beam is called the *zone of silence* [28]. The supersonic beam continues to expand until the pressure in the beam is less than the pressure p_0 in the surrounding medium. At this point, the beam is said to be *overexpanded* [28, 29]. Due to the pressure difference, the beam starts to contract in oblique shock waves called the *barrel shock* [28, 29]. The barrel shock changes the flow direction and the Mach number until the flow becomes sonic. The compression of the beam increases its pressure until the starting pressure p_e is reached in the Mach disk. At this point the beam is underexpanded and the expansion and increase of Mach number may repeat.

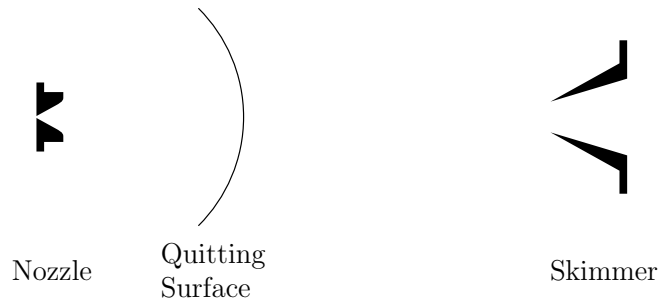


Figure 2.3: Flow-field of the underexpanded flow from a diverging nozzle. The figure shows conceptually the location of the quitting surface, the surface that delimits the continuous from the molecular flow regime, and the placement of the skimmer.

For very low ambient pressures, this picture must be modified. As the

beam expands and its pressure and density decrease, the distance of the Mach disk from the nozzle increases and the barrel shock becomes thicker [28, 29]. At low enough pressures, this diffuse shock is replaced by a region of scattering between particles of the nozzle beam and the background gas. This transition happens gradually if the mean free path after the Mach disk is long enough. Upstream of this transition, the particles in the beam behave as a continuous gas and downstream the particles collide very rarely and the beam becomes molecular [28]. In theoretical considerations, this transition is often assumed to be abrupt, such that the transition between the continuous flow and the molecular flow happens on a spherical surface called the *quitting surface* (see figure 2.3). This treatment is called the *sudden freeze approximation* [28], as internal degrees of freedom "freeze" downstream of this transition due to the lack of collisions.

As the gas rarefies and collisions become less important, the notion of the sound speed loses its physical meaning. Therefore the Mach number is often replaced by the speed ratio $S = \bar{v}/v_t = \sqrt{\kappa/2}M$, where \bar{v} is the flow velocity of the beam and v_t is the most probable thermal velocity of particles inside the beam [29, 28].

As the beam moves down the beamline, its velocity distribution becomes narrower due to collisions between particles that reduce the velocity spread v_t . However, further downstream, collisions also become less likely such that the beam approaches a terminal speed ratio S_∞ corresponding to a terminal temperature T_∞ [28, 29]. The terminal temperature can be as low as

10^{-3} K [29]. The cooling of the beam that is achieved in this way is referred to as *translational cooling*. Note that due to the low number of collisions at large distances from the nozzle, the parallel and transverse spatial directions are no longer in thermal equilibrium and reach distinct temperatures T_{\parallel} and T_{\perp} , due to different cooling mechanisms [28].

In fact, the transverse temperature T_{\perp} experiences an additional geometric cooling effect. Particles with similar transverse velocities v_{\perp} are spatially aligned, as they spread at similar rates from the center of the beam. As the beam expands further, the transverse velocity distribution in a volume element thus becomes narrower. The maximum rate of geometric cooling is $T_{\perp} \propto x^{-2}$, where x is the distance from the nozzle [28]. This effect is strongly reduced in the parallel direction [28].

The colder part of the beam close to the axis can be selected using a skimmer, which is a conical or wedge shaped diaphragm (see figure 2.3). If the background pressure is high, the skimmer should be placed close to the nozzle in the zone of silence penetrating the Mach disk [28]. If the background pressure is low enough, so that molecular flow is achieved (such as in our system), then the skimmer should be placed after the quiting surface, to achieve better collimation and cooling as well as a greater speed ratio [29].

The skimmer can also have disadvantageous side effects. For high enough flux in front of the skimmer, particles that are reflected back from the skimmer walls can act as scattering targets for the incoming beam. This phenomenon is known as *skimmer interference* and happens even if the skim-

mer is placed after the quiting surface in the molecular flow regime [28]. At higher flux, this scattering region develops into a diffuse shock, which at even higher flux is pushed downstream and forms an oblique shock along the skimmer edges and causes flow disturbances inside the skimmer [28]. At lower pressures, background gas may penetrate through the skimmer and scatter the beam after it has passed through the skimmer [28]. All these effects cause a reduction in flux of the molecular beam across the skimmer [28] that can be as large as two orders of magnitude [26].

The placement of the skimmer thus has significant influence on the quality of the beam, but it can facilitate the creation of a much colder and better collimated molecular beam.

2.2 Beam Simulation using Direct Simulation Monte Carlo (DSMC)

A possible way of approaching the behavior of the supersonic beam is through numerical simulations. A method for simulating the flow of rarefied gases outside of the continuous regime is given by the *Direct Simulation Monte Carlo* (DSMC) method [30, 31, 32, 33]. This section will give an overview of this method and present some simulation results.

The mathematical model to describe the flow of a dilute gas is given by the Boltzmann equation [32, 33]. Let \vec{X} be the position in space and \vec{V} be the molecular flow velocity in the flow-field. The physical parameters of the system such as number density ρ , flow velocity \vec{v} , temperature T , pressure

p , etc can be expressed as the moments of the *velocity distribution function* $f(\vec{X}, \vec{V}, t)$ [32]. The behavior of the velocity distribution function is governed by the Boltzmann equation [32]:

$$\frac{\partial f}{\partial t} + \sum_{i=1}^3 V_i \frac{\partial f}{\partial X_i} + \sum_{i=1}^3 \frac{\partial F_i f}{\partial V_i} = J(f, f) \quad (2.1)$$

The second term describes the movement of the gas due to the molecular velocity \vec{V} , the third term describes changes in the velocity due to an external force \vec{F} and the right hand side describes inter-molecular collisions [32].

Instead of solving the Boltzmann equation directly, the DSMC method utilizes a probabilistic approach that embodies the same assumptions that yield the Boltzmann equation [32, 33].

In the DSMC method, a group of $N_{\vec{v}, \vec{x}}$ of real particles in the dilute gas with roughly the same velocity \vec{v} and position \vec{x} are represented in the simulation by a single particle with \vec{x} and \vec{v} . The particles in the simulation are thus a representation of a much larger number of real particles in the dilute gas [32, 33].

The finite spatial domain of the simulated flow is initially divided into a set of cells with index l that do not change over the course of the simulation. Given an initial set of simulation particles with given positions and velocities \vec{x} and \vec{v} , the time evolution of the particles can be calculated in time steps Δt by repeating the following three steps [32, 33]:

Step 1 Evolve the positions $\vec{x}_{j,l}$ of all particles j in every cell l , by letting the particles move with their velocity $\vec{v}_{j,l}$ for the duration of the timestep

Δt . The velocity is then changed to represent the action of the external force \vec{F} during Δt . During this process, a particle may enter a different cell. It will then be associated with that new cell, i.e. $l \rightarrow l'$.

Step 2 Particles that leave the simulation domain are removed and new particles are added at boundaries with flow into the simulation domain.

Step 3 In every cell l , pairs of particles are selected probabilistically. The velocities $\vec{v}_{j,l}$ of the particles in a pair are then changed to mimic the effect of binary collisions.

These three steps are repeated successively to simulate the evolution of the gas over time. The physical parameters of the gas can be calculated from the positions $\vec{x}_{j,l}$ and velocities $\vec{v}_{j,l}$ of the particles, which take a role analogous to the velocity distribution function f in the Boltzmann equation.

It can be shown that the DSMC method in its simplest form is a solution of the Boltzmann equation [34, 32]. However, the method is flexible enough to account for mechanism such as chemical reactions and radiation emission that are difficult to treat in the Boltzmann equation [33].

I applied the DSMC method to learn about the supersonic nozzle that we use. To this end, the software programs *DS2V* [33] and *SPARTA* [35, 36] have been used. DS2V is a standard tool written by G. Bird who originally proposed the DSMC method [30]. Sparta is a highly parallelized DSMC solver developed at Sandia by S. Plimpton and M. Gallis at Sandia National Laboratories and was chosen for its faster performance. The nozzle in the simulations

shown below has a length of 7.6 mm, a half-opening angle of 40° , an aperture diameter of $200\ \mu\text{m}$, and it is held at a temperature of 165 K. The gas is helium with a stagnation pressure of 3 bar. Higher pressures have not been attempted due to the increasing cost in simulation time.

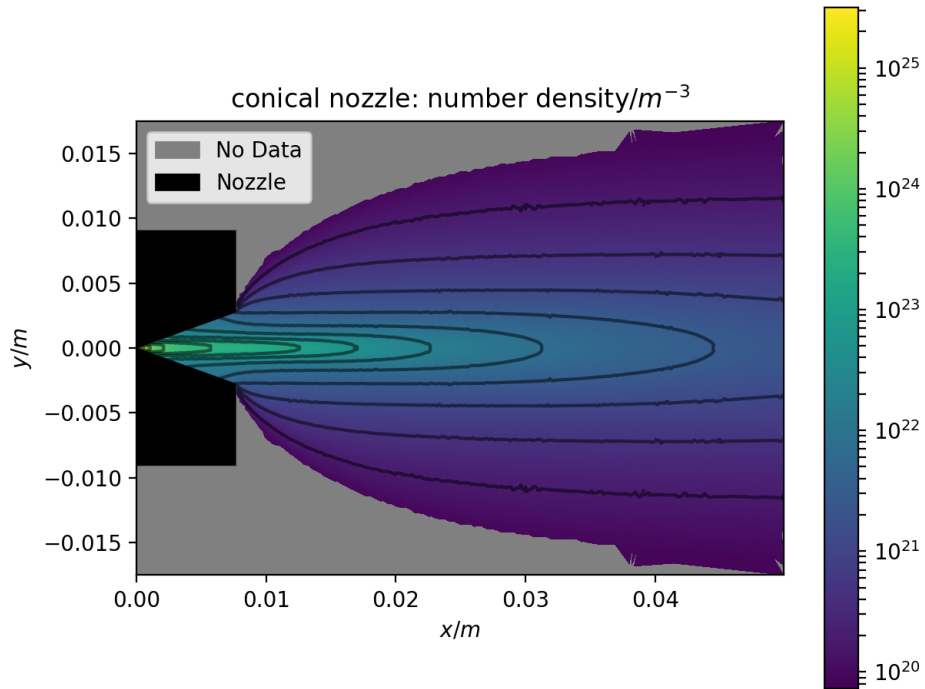


Figure 2.4: Number density in the flow-field in a conical nozzle. The flow is anisotropic, favoring the forward direction along the nozzle axis, as seen from the elongated arcs in the contour lines.

Figures 2.4, 2.5 and 2.6 show the number density ρ , the Mach number M and the temperature T of the beam, respectively. The results compare well to the ones shown in [27] and [26]. The beam becomes supersonic well inside the nozzle. There is some interaction with the nozzle walls as seen by layer

of higher temperature and lower Mach number. The flow in the center of the nozzle however quickly gains higher Mach numbers and stays cold.

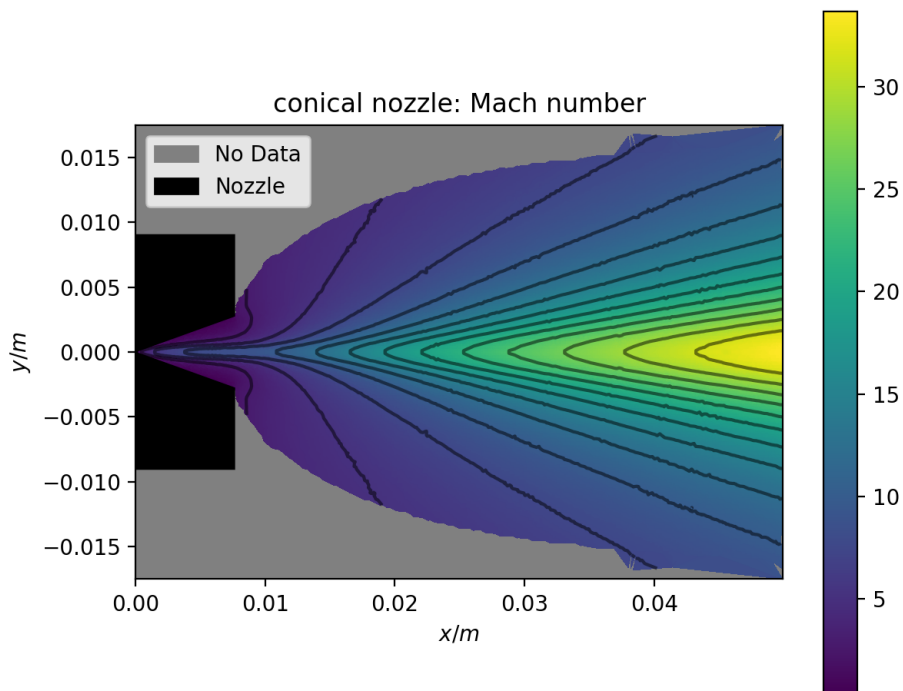


Figure 2.5: Mach number in the flow-field in a conical nozzle. Inside the nozzle, close to the walls, there are collisions with the walls that slow the beam, however, close to the axis of the nozzle the beam quickly becomes supersonic. Once outside the nozzle, the beam becomes highly supersonic.

As the stream exits the nozzle, it adapts to the new boundary condition by expanding in the direction normal to the propagation. Note that these simulations do not consider a background gas of finite pressure and so the results are only valid in the region close to the nozzle and the center of the beam, where the flow is largely unaffected by interactions with the background

gas.

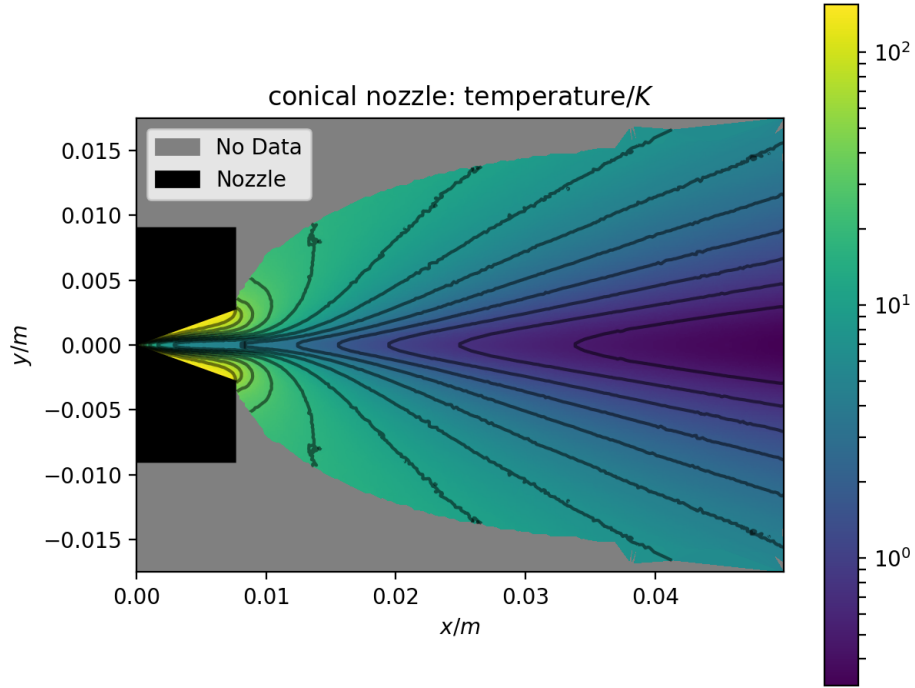


Figure 2.6: Temperature in the flow-field in a conical nozzle. Inside the nozzle, off of the central axis the beam is heated due to collisions with the nozzle walls, however the flow near the center of the nozzle stays cold. After exiting the nozzle the beam expands and cools significantly.

As seen in figures 2.5 and 2.6, the beam, after exiting the nozzle, quickly becomes highly supersonic and very cold. Also, the emission in terms of number density is anisotropic, strongly favoring propagation along the nozzle axis as seen from the strongly elongated contour lines of the number density (figure 2.4).

These beam properties are very beneficial to our experiment, as a cold

beam with high number density in the forward direction is desired to achieve a high enough density and low divergence downstream where entrainment would take place.

Chapter 3

Methods for Entraining Lithium and the Idea of the Recirculating Oven

3.1 Effusive Oven

There are several methods to achieve the entrainment of a payload species into a pulsed supersonic beam [25]. The simplest method is to use an oven loaded with the payload material in the vicinity of the supersonic beam.

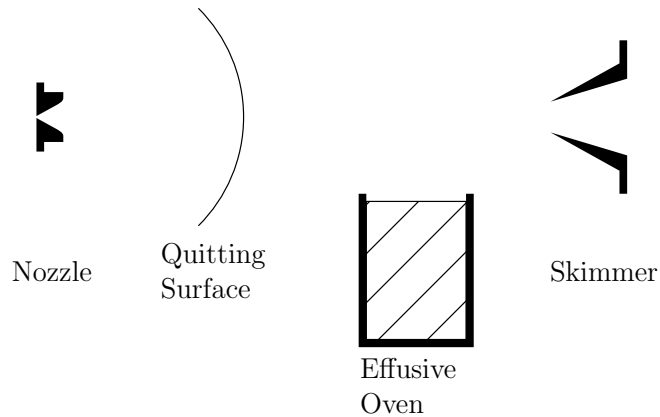


Figure 3.1: Conceptual drawing of the effusive oven in the supersonic beam line. The oven consists of a heated reservoir containing the lithium payload. The oven is open to vacuum at the top allowing the lithium to escape into the chamber volume and entrain into the supersonic beam.

A conceptual drawing of such an oven is shown in figure 3.1. The oven consists of a heated reservoir containing a payload material (lithium). The

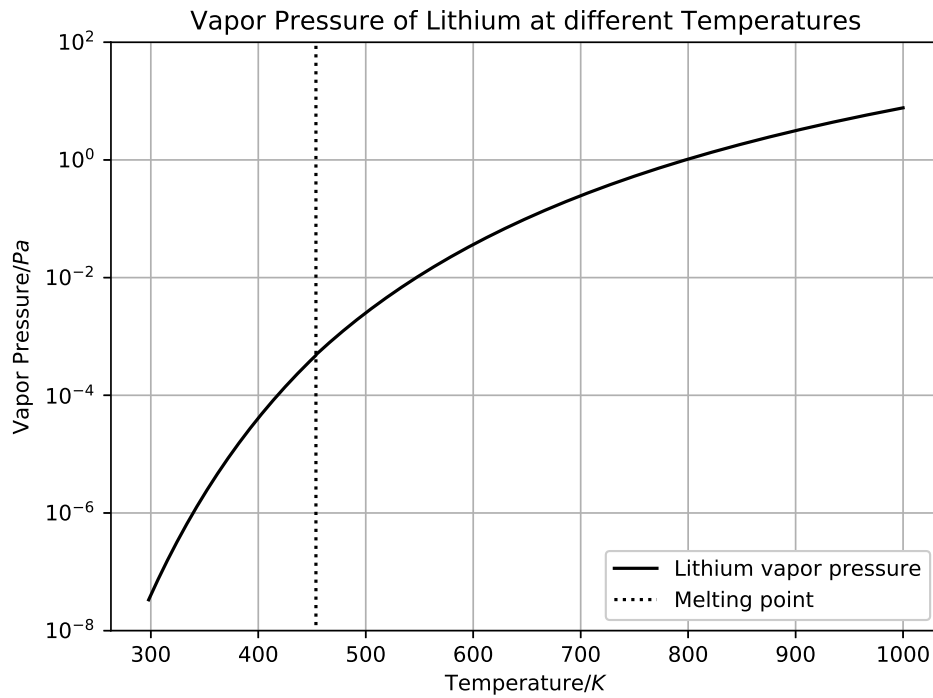


Figure 3.2: Vapor pressure of lithium as a function of temperature. The dotted line indicates the melting point of lithium. The vapor pressure increases and surpasses the ambient pressure of 10^{-7} torr (10^{-5} Pa) at about 370 K before it liquefies. The vapor pressure increases further to the order of 1 Pa at 900 K. Data from [37].

lithium will be heated in the reservoir container to several hundred degree Celsius to the point where the vapor pressure of the payload material in the reservoir greatly surpasses the ambient pressure and individual atoms leave the surface of the material and penetrate into the vacuum chamber. For lithium, temperatures of 450 °C to 700 °C are sufficient to create high vapor pressures [37, 38] as shown in figure 3.2. The atoms that are sprayed off the payload material surface will travel in any direction and will also penetrate the supersonic beam where they are entrained into the flow through collisional equilibration.

The disadvantage of this method is the fact that the oven sprays the payload in all directions which results in a lot of the lithium getting lost in the vacuum chamber without ever reaching the supersonic beam. This leads to a short lifetime of the reservoir since a high total flux of atoms out of the oven has to be maintained in order to keep the flux of lithium atoms into the supersonic beam reasonably high. This disadvantage leads to quick depletion of the oven reservoir and contamination of the vacuum chamber. This requires the chamber to be frequently opened to refill the oven and thus interferes with the experiment.

3.2 Directional Oven

The disadvantage of the short lifetime of an effusive oven may be limited by an oven design with a capillary nozzle which creates a directional beam of lithium atoms [39].

To achieve directionality in the spraying behavior of the oven, the open-

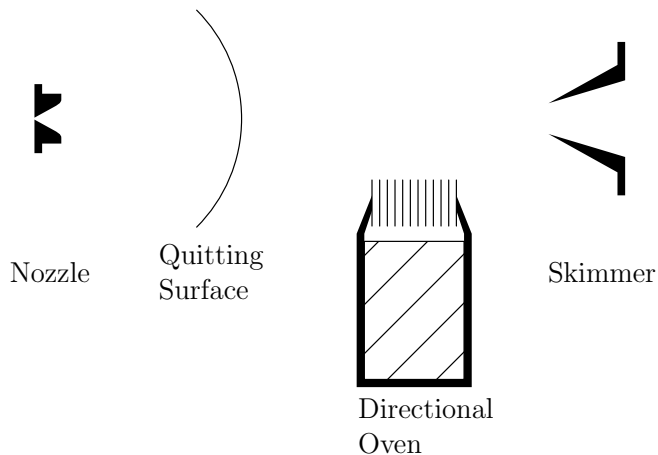


Figure 3.3: Conceptual drawing of the directional oven in the supersonic beam line. The top opening of the oven is filled with an array of micro-capillaries, which only allow lithium atoms to escape if their trajectories are aligned with the axis of the micro-capillary array.

ing of the reservoir through which the lithium atoms escape is stacked with micro-capillaries. These are small tubes of a length of several centimeters and a diameter of several $100\ \mu\text{m}$. A conceptual drawing of this geometry is shown in 3.3.

The lithium atoms can only traverse this layer of micro-capillaries if their direction of travel coincides with the cylindrical axis of the capillaries within a small margin of error. If this condition is not satisfied the lithium atoms will collide with the inner walls of the capillaries and can not escape into the vacuum chamber, but will instead be returned into the reservoir [39]. The resulting beam of lithium atoms is therefore aligned with the axis of the capillaries and can be used to spray lithium into the supersonic beam with only minimal flux being lost in other directions.

Due to the better targeting this oven can be run at lower temperatures, which increases the lifetime of the lithium reservoir. When operated at higher temperatures, it eventually loses directionality as the mean free path of the lithium atoms in the vapor becomes comparable to the diameter of the capillaries. The flux that can be obtained from this oven in the regime of directional emission is thus limited.

Another disadvantage of this oven and the use of an oven in general is that it emits atoms continuously. However, since the supersonic beam is pulsed, a lot of the lithium atoms will be emitted when there is no supersonic beam to penetrate and will therefore be lost.

3.3 Flashed Ribbons

The lithium emission can also be targeted to the supersonic beam in the time domain by using a metal ribbon mounted above the supersonic beam on axis with the directional oven [25].

As shown in figure 3.4, the large planar surface of the ribbon directly faces the oven. During the time at which the supersonic beam is switched off, the payload particles emitted by the oven will hit the surface of the ribbon and stick to it. Thus, a layer of lithium is accumulated on the ribbon. By pulsing a current of several hundred amperes through the ribbon that was dosed with lithium in this way, the ribbon can be heated and the lithium can be released. If this current pulse in the ribbon is synchronized with the Even-Lavie valve then all of the accumulated lithium will penetrate the supersonic beam and

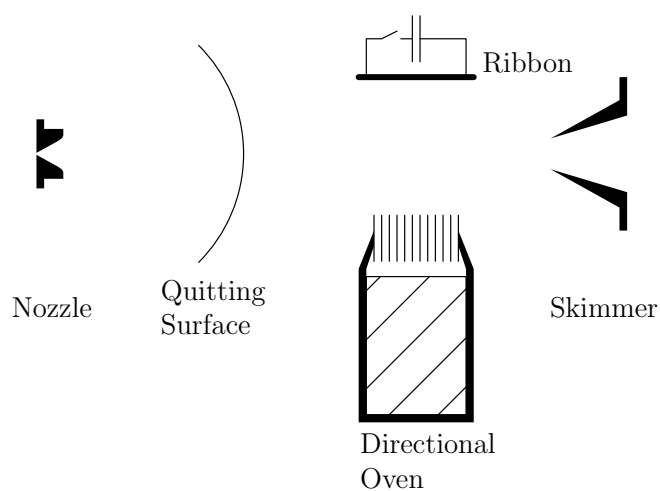


Figure 3.4: Conceptual drawing of the directional oven loading the ribbon. The ribbon is mounted above the oven so that the supersonic beam passes in between them. The oven constantly deposits lithium on the ribbon, which can be flashed off of the ribbon by pulsing current. This allows us to synchronize the lithium release with the passing of the supersonic beam.

possibly entrain.

The use of the ribbon therefore complements the directional oven to not only target the supersonic beam more accurately in the spatial domain, but also in the time domain to maximally reduce the loss of payload particles into the vacuum chamber. It thus significantly reduces the required oven flux by directing it more efficiently into the supersonic beam. The oven can thus be comfortably run at temperatures where its emission is highly directional. The lifetime of the oven reservoir is therefore increased, making interruptions of the experiment less frequent.

One disadvantage of the ribbon design is the fact that the ribbon needs a finite time to cool and re-accumulate lithium after a pulse. Because of this, the repetition rate is limited to less than a few hertz.

3.4 Recirculating Oven: The Heat Pipe

One of the disadvantages of both the effusive and the directional oven is the loss of all emitted lithium atoms that do not get entrained into the supersonic beam. In both cases the pulsed supersonic beam only passes through the continuously emitted lithium vapor for a very short time (up to tens of microseconds at a repetition rate on the order of 1 Hz). All the lithium that is not entrained into the supersonic beam is lost in the vacuum chamber and deposits on the chamber walls. An obvious improvement would be to capture all lithium that is not entrained and recirculate it into the oven to increase oven lifetime.

Recirculating ovens for the direct formation of molecular beams of various materials have been used before [40, 41, 42, 43], however, we propose to use this idea in an oven that is specifically designed for entrainment into a supersonic beam of a light carrier gas and not for the direct emission of a molecular beam from the oven.

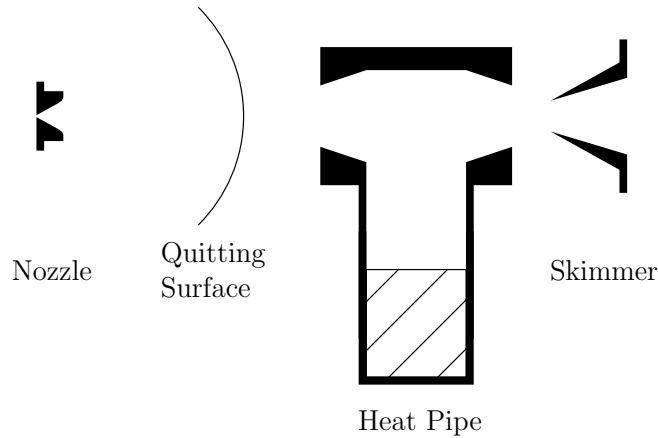


Figure 3.5: Conceptual drawing of the "heat-pipe" recirculating oven and its position in the path of the supersonic beam: The oven consists of a heated cylindrical reservoir partially filled with liquid lithium (hatched). The lithium that evaporates in the reservoir emerges into the cylindrical beam head, which is aligned with the propagation direction of the supersonic beam. lithium is then either entrained or deposited on the beam head walls, as the geometry is chosen such that there is no direct line of sight from the lithium in the reservoir to the exit holes of the beam head. The lithium on the walls is recirculated into the reservoir through gravity and capillary action.

A conceptual drawing of the proposed oven is shown in figure 3.5. Lithium (hatched) is stored in a long cylindrical reservoir tube that can be heated to high enough temperatures (up to 900 K) to create a significant lithium vapor pressure. However, the temperature is chosen to be low enough

so that the lithium vapor is in the non-collisional regime and behaves as an atomic beam. Thus, the lithium beam that emerges from the partially filled reservoir tube is confined to a known solid angle. As it emerges from the reservoir, the lithium enters another cylindrical tube mounted perpendicular to the reservoir called the beam head, such that its axis is aligned with the propagation direction of the supersonic helium beam. The helium beam can thus enter the beam head through its front orifice, propagate through it and entrain lithium, before finally exiting out of the back orifice. The length of the cylindrical tube of the beam head is chosen long enough such that there is no line of sight from the surface of the liquid lithium in the reservoir out of the openings of the beam head. Thus all the lithium that is emitted from the reservoir is either entrained into the supersonic helium beam or it collides with the beam head walls.

The beam head is kept at temperatures above the melting point of lithium (180.50 °C [37]) but significantly lower than the reservoir to minimize the vapor pressure of the accumulating lithium to avoid secondary emission, which would be in line of sight with the openings of the beam head and would thus lead to lithium loss to the vacuum environment. The lithium that is not entrained is thus captured on the beam head walls and forms liquid puddles that can be recirculated into the reservoir.

The obvious force driving this recirculation is gravity. However the force driving the lithium back into the reservoir can be increased by layering the inside of the beam head and the reservoir with a material with fine patterned

structure such as a wire mesh or capillary tubes or grooves. The liquid lithium can wet these structures and recirculate to the reservoir through capillary action. This concept has been used e.g. in [44, 45].

The principle of evaporation at a hot surface and condensation at a colder surface and subsequent recirculation through capillary action is widely used for efficient heat transport [46, 47]. In this context, a system like this is called a *heat pipe* for transporting heat like a pipe [46, 47]. As the recirculation in our oven uses the same principal, we borrow this name to describe this aspect of our oven.

Chapter 4

Measurement Techniques

4.1 Residual Gas Analyzer

To detect the supersonic helium beam we use a residual gas analyzer (RGA) (see e.g. [48]) . The model used is a *RGA200* from Stanford Research Systems [49].

An RGA consists of an ionizer and a quadrupole mass spectrometer. As shown in figure 4.1, neutral helium atoms traveling in the supersonic beam are ionized by electron-bombardment from a incandescent filament. The ions are accelerated by a voltage between the anode grid and the focus plate to an energy of 12 eV [49]. After this acceleration, the ions enter a quadrupole mass spectrometer, which is used as a mass filter by applying a constant frequency matching the specific charge of singly ionized helium atom to the quadrupole rods. At the end of the quadrupole filter, the ions are collected and the ion current is determined using a Macro Multi-Channel Continuous Dynode Electron Multiplier (CDEM). The CDEM signal is amplified by a current preamplifier (FEMTO DHPA-100) and a voltage amplifier (SRS Model SR560) and then measured as a function of time using a National Instruments PCI-6133 data acquisition system. In this way, a relative measurement of the number of he-

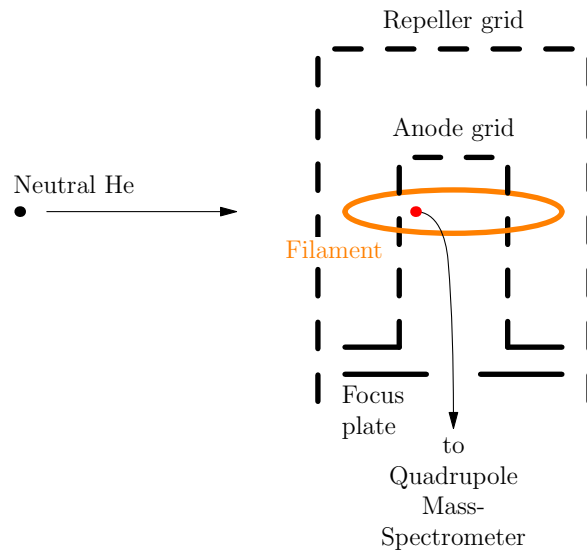


Figure 4.1: Illustration of the method of operation of a residual gas analyzer. The heated filament emits electrons that are accelerated towards the anode grid. Neutral atoms that enter the anode grid are bombarded with electrons and ionized. They are then accelerated away from the anode grid and towards the focus plate. After transmission through the hole in the focus plate, the ions enter the quadrupole mass spectrometer.

lithium atoms passing through the detector as a function of time can be obtained with a temporal resolution of $0.4 \mu\text{s}$.

In our vacuum system, the RGA is mounted such that the axis of its quadrupole spectrometer is perpendicular to the propagation direction of the supersonic helium beam. The helium atoms thus have a velocity component perpendicular to the spectrometer axis in the order of several hundred meters per second. This velocity component does however not influence the collection efficiency or the fidelity of the mass spectrometer significantly as the atoms receive a velocity component along the spectrometer axis of $24 \times 10^3 \text{ m/s}$ due to the voltage on the anode grid accelerating the ions to 12 eV [49]. After that, the propagation direction of the ions is aligned to the spectrometer axis within an error of less than 3° , which the quadrupole filter can tolerate. Mounting the RGA perpendicular to the supersonic beam thus does not influence its operation significantly.

4.2 Langmuir-Taylor Detector

The detector that we use to measure time of flight signals of the lithium content of our beam is based on the principle of surface ionization. If an atom approaches a metal surface close enough, electrons may be exchanged between the atom and the surface via the tunnel effect. The direction of this exchange and its probability are dependent on the work function Φ , i. e. the energy it takes to remove one electron from the surface, as well as the ionization energy I or the electron affinity A of the atom, for positive or negative ions respectively

[29]. The efficiency of ionization is given by the ratio of the number of ions i_{\pm} that leave the surface to the number of atoms $i_{\pm} + i_0$ that strike the surface initially. This ratio is given by the *Saha-Langmuir* equation [29]:

$$\frac{i_{\pm}}{i_{\pm} + i_0} = \left(1 + \frac{g_0}{g_{\pm}} e^{\Delta U/(kT)} \right)^{-1} \quad (4.1)$$

$$\Delta U = I - \Phi - e\sqrt{eE}, \quad \text{for positive ions}$$

$$\Delta U = \Phi - A - e\sqrt{eE}, \quad \text{for negative ions}$$

Here, g_{\pm} and g_0 are degeneracies in the ionic and in the atomic state. For alkali atoms, $\frac{g_0}{g_{\pm}} = 2$ [50]. The efficiency of the ionization can be influenced by applying an external electric field E . For alkali metals, ionization efficiencies close to 100% can be achieved.

For detection purposes, the surface is kept at elevated temperatures, so that the ions evaporate off. By applying a voltage between the ionization surface and some collector, the ions can be collected and their number can be measured as the current between the collector and the ionization surface. Since the ionization at the surface happens very fast ($< 0.1 \mu\text{s}$ [51]), the detector has the required temporal resolution for time of flight measurements [51].

To detect lithium, which has the highest ionization energy of the alkali atoms with $I = 5.392 \text{ eV}$ [50], we use a rhenium ribbon [52], which has a work function of $\Phi = 4.96 \text{ eV}$ [50]. The rhenium ribbon is heated resistively to incandescence and a bias of 12 V is applied with reference to the collector. The ion current is measured using a current preamplifier (FEMTO DHPKA-100) and a voltage amplifier (SRS Model SR560) and the same National Instru-

ments PCI-6133 daq system that is used for the RGA as well, which allows to accurately reference the two signals to each other in time.

The rhenium ribbon and the collector are mounted in a cage such that the beam passes through an open surface in the collector, interacts with the ribbon, and passes out of the collector behind the detector. The ribbon is mounted vertically, normal to the propagation direction of the beam and the whole sensor can be translated horizontally, to scan the beam along its transverse extent and measure its width and profile.

4.3 Optical Resonant Absorption

4.3.1 Overview

To measure the lithium content entrained in the supersonic beam, we use optical absorption in a laser beam tuned to the lithium $D2$ line.

A schematic of the optical system that creates the tuned laser is shown in figure 4.2. A diode laser (Toptica Diode pro) is locked to the lithium 7 $D2$ transition using Doppler-free spectroscopy (saturated absorption spectroscopy [53, 54, 55, 56]) in a lithium vapor cell. This laser is used to seed a tapered amplifier (Toptica TApro). The amplified laser is then frequency-shifted using two acousto-optical modulators (AOM) to correct for a frequency offset acquired in the locking of the tapered amplifier to the seed laser using a beat-locking technique [57]. The AOMs also allow us to generate 2 different arbitrary frequency detunings from the $D2$ transition to correct for the Doppler-shift in the moving frame of the supersonic beam and to arbitrarily detune from resonance

for off-resonance spectroscopy. The two frequencies are distinguished by their polarization.

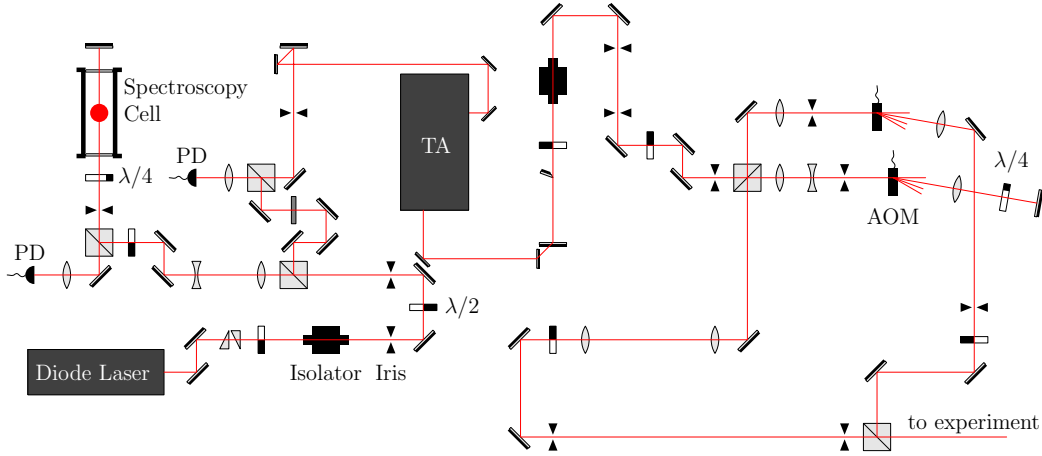


Figure 4.2: Schematic of the optical setup for generation of a 670 nm laser tuned to the lithium $D2$ line. The diode laser is locked to a spectroscopy cell using saturated absorption spectroscopy. The frequency reference obtained in this way is then used to lock the tapered amplifier (TA) using a beat-locking technique. The offset acquired in the beat-locking is removed in the two acousto-optical modulators (AOM), which also allow to create two different arbitrary detunings to target different Doppler-shifted velocity groups. $\lambda/2$: half-wave plate, $\lambda/4$: quarter-wave plate, PD : Photodiode.

The laser that has been tuned to the lithium $D2$ line in this way is then directed through the vacuum system, perpendicularly intersecting the trajectory of the supersonic beam. There, part of the beam power is absorbed and reemitted isotropically, leading to a loss of laser power proportional to the number of lithium atoms in the beam path. The laser power is then measured with a photodiode. The dip in the signal from the photodiode contains information of the arrival times, beam shape, and relative number of lithium atoms

entrained in the supersonic helium beam.

4.3.2 Saturated Absorption Spectroscopy

We use saturated absorption spectroscopy to remove the Doppler broadening of the signal in the vapor cell. This technique utilizes two beams that propagate in opposite directions and cross inside the vapor cell. The beams are called *pump beam* and a *probe beam* [54, 55, 56]. In this setup, we use the the Toptica DL100 as pump beam. Before entering the vapor cell, it passes through a $\lambda/4$ plate at 45° to the polarization axis of the beam. It then passes through the vapor cells in circular polarization, before it is reflected back on itself by a mirror. We use this reflected beam as probe beam. After passing the vapor cell, it passes through the $\lambda/4$ plate a second time, which makes it linearly polarized, with a total rotation of its polarization axis of 90° . With this rotation, it passes through the polarizing beamsplitter cube to the photodiode.

The lithium vapor in the spectroscopy cell is held at a temperature of 400°C . The velocities of the individual atoms follow a Maxwell-Boltzmann distribution [54]. At this temperature, absorption can be observed in a wide frequency band (GHz) around the true resonance frequency of the lithium D2 line ($\lambda = 670.8\text{ nm}$ [37]) due to the large velocity spread. The atoms with resonance frequency ω in their rest frame travel at some velocity \vec{v} in the vapor in the cell, which shifts their resonance as seen by a laser of wavevector \vec{k} to $\omega' = \omega - \vec{k} \cdot \vec{v}$.

Let the frequency of the pump beam be a little off of the rest frame

resonance frequency ω at ω_1 . It will then excite atoms with a velocity \vec{v}_1 that satisfies $\omega_1 = \omega - \vec{k}_1 \cdot \vec{v}_1$. After reflection at the mirror at the other end of the cell, the beam, now considered the probe beam, travels in the opposite direction, i.e. with $\vec{k}_2 = -\vec{k}_1$. Thus, it excites atoms with a velocity that fulfills the condition $\omega_1 = \omega + \vec{k}_1 \cdot \vec{v}_2$. Thus a laser that is detuned from the resonance ω will be absorbed in two different velocity groups before and after reflection.

We really want the frequency of the laser to match the resonance frequency in the rest frame, i.e. we want $\omega_1 = \omega$, which implies $\vec{k}_2 \cdot \vec{v}_2 = \vec{k}_1 \cdot \vec{v}_1 = 0$. This means that at ω , the probe and the pump beams are resonant with atoms that are at rest in the direction parallel to the beam. Coincidentally, this also means that the probe and pump beams would interact with the same group of atoms, which is not the case if the laser is detuned.

Experimentally, it can be detected if the two counter-propagating beams are on resonance with the same group of atoms. When the pump beam passes through the vapor, it is absorbed in atoms of a particular velocity group, which reduces the laser power measurably and excites the atoms to a different state. If the laser is detuned, the probe beam acts in the same way on a different velocity group and the beam loses power a second time. However if the laser frequency matches the resonance frequency in the rest frame, the velocity groups coincide.

In this case however, the probe beam no longer interacts with the lithium atoms in the vapor because the transition is already saturated by

the pump beam. This leads to a peak in the transmitted laser power as a function of laser frequency exactly when the laser frequency coincides with the resonance frequency of the atoms. The width of this peak in frequency is the natural linewidth (5.9 MHz [37]) of the transition and is not Doppler broadened. It can be used to precisely lock the laser.

Chapter 5

Heat Pipe Entrainment behind the Skimmer

5.1 Design of the Heat Pipe

The first design for a heat pipe oven that was tried is the one presented in [25]. It consists of a cylindrical tube (beam head) with its axis parallel to the propagation direction of the supersonic beam and a reservoir that contains lithium and can be heated externally. The reservoir is mounted perpendicularly onto the beam head (see figure 5.1). The whole structure is mounted behind the skimmer and serves as vacuum vessel, i.e. its outside surface is exposed to ambient pressure.

The beam head is 8" long along its axis, and it has an inner diameter of 1.420" and an outer diameter of 1.500" at the ends. Both ends are fitted with a standard 2.75" conflat flange for connection to the rest of the vacuum system. At its center, the outer diameter of the beam head increases to 2.500" over a length of 4.250". In this region, the inner walls are sloped and reach an inner diameter of 1.950" at their widest point, at which the reservoir is attached perpendicularly to the bottom of the beam head (see figure 5.2). The thicker walls of the beam head in this region serve as a thermal mass with the purpose to keep this region at elevated temperatures, so that the lithium

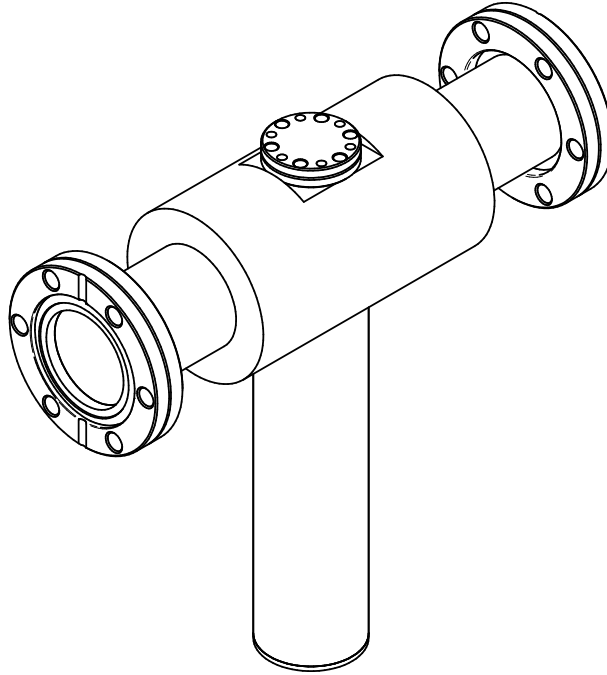


Figure 5.1: Conceptual drawing of the heat pipe. It consists of a tube (beam head) that is aligned with the propagation direction of the supersonic beam. The heat pipe is mounted behind the skimmer using the 3.75" CF-flange on both ends. In the middle, the reservoir is attached to the bottom of the beam head. It consists of a cylindrical tube that contains the lithium and can be heated externally.

that accumulates in here stays liquid and can be recirculated back into the reservoir. Close to the flanges, the walls of the beam head are thin, to hinder thermal conduction and keep the flanges cool.

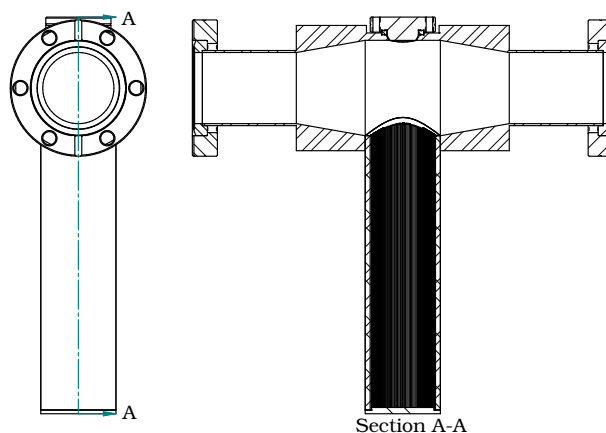


Figure 5.2: Drawing of a cross section through the heat pipe along the propagation axis of the supersonic beam. The beam head has thick walls near the center that act as thermal mass to keep the temperature elevated in this region. Close to the flanges, it is thin to minimize heating of attached chambers and, in particular, the skimmer. The reservoir is lined with 160 grooves parallel to its axis. These grooves are 0.015" wide and 0.02" deep and enhance the recirculation of the lithium through capillary action.

The reservoir is a cylindrical tube that is mounted perpendicularly on the center of the beam head, which places it 8" behind the opening of the skimmer and 12" from the supersonic nozzle. It measures 6.500" from the central axis of the beam head to its foot and has an inner and outer diameter of 1.250" and 1.500", respectively. During operation, it is loaded with 25 g of lithium and heated externally using heater tape or cartridge heaters.

The inside walls of the reservoir are fitted with 160 small grooves that

run parallel to its axis. These grooves 0.020" deep and have a diameter of 0.015". They have been cut using an electric discharge machine [48]. Their purpose is to aid in the recirculation of the lithium into the reservoir through capillary action. The liquid lithium that accumulates in the beam head wets the capillaries. Due to its surface tension ($\sigma = 0.386 \text{ N/m}$ [58]) the liquid lithium then experiences a pressure of $P = 2\frac{\sigma}{r} = 4 \times 10^3 \text{ Pa}$ or 30 torr [44] that wicks the lithium into the grooves where it flows back to the bottom part of the reservoir and can be reemitted. This approach to recirculation using capillary action has been implemented before e.g. in [44]. Due to the larger surface tension of liquid lithium [58], the machined grooves are sufficient in this case and we do not need to use finer materials like wire meshes.

5.2 Controlling Hydrogen Desorption

The original heat pipe as proposed in [25] was machined from stainless steel 316. This turned out to be problematic due to high pressures resulting from hydrogen desorption.

Stainless steel contains large amounts of absorbed hydrogen that is dissolved within its structure. With increasing temperature, this hydrogen can be released which results in an additional pressure load on the vacuum system. This phenomenon is known as hydrogen desorption and is a well studied problem in vacuum technology [59, 60, 61, 62, 63] In particular this is a problem for the heat pipe due to its relatively confined volume and the skimmer, which reduces pumping speed in this part of the chamber system.

One factor leading to the high hydrogen desorption in the heat pipe is the interaction of the steel with the liquid lithium. Liquid lithium generally corrodes steel. The corrosion then exposes the volume of the steel and makes hydrogen diffusion to the surface easier and thus yields more hydrogen desorption. Austenitic steels such as the grade 316 steel [64] suffer from corrosion to a higher degree than ferritic steels [65]. To limit corrosion we thus constructed another heat pipe with identical design from the ferritic steel of grade 430.

Corrosion of the steel can also be reduced by baking the heat pipe at temperatures below the melting point of lithium, to remove water and hydrogen from the steel surface. In the presence of water and hydrogen, lithium can form different lithium hydride which is highly corrosive. This reaction can be suppressed by removing water and hydrogen from the steel surface by baking at 150 to 200°C.

We measured the pressure levels in the vacuum system with the reservoir held at different temperatures with the heat pipes made from 316 and 430 steel. The results are shown in figure 5.3. When using the 316 steel, the pressure at temperatures of 400°C to 600°C is roughly an order of magnitude higher than the pressure with the 430 steel heat pipe. Due to this lower pressure, grade 430 stainless steel has been used in all further experiments.

5.3 Effects on the Helium Beam and Entrainment

The entrainment process depends on the density of the lithium vapor that is produced in the beam head of the heat pipe. To find a good operating

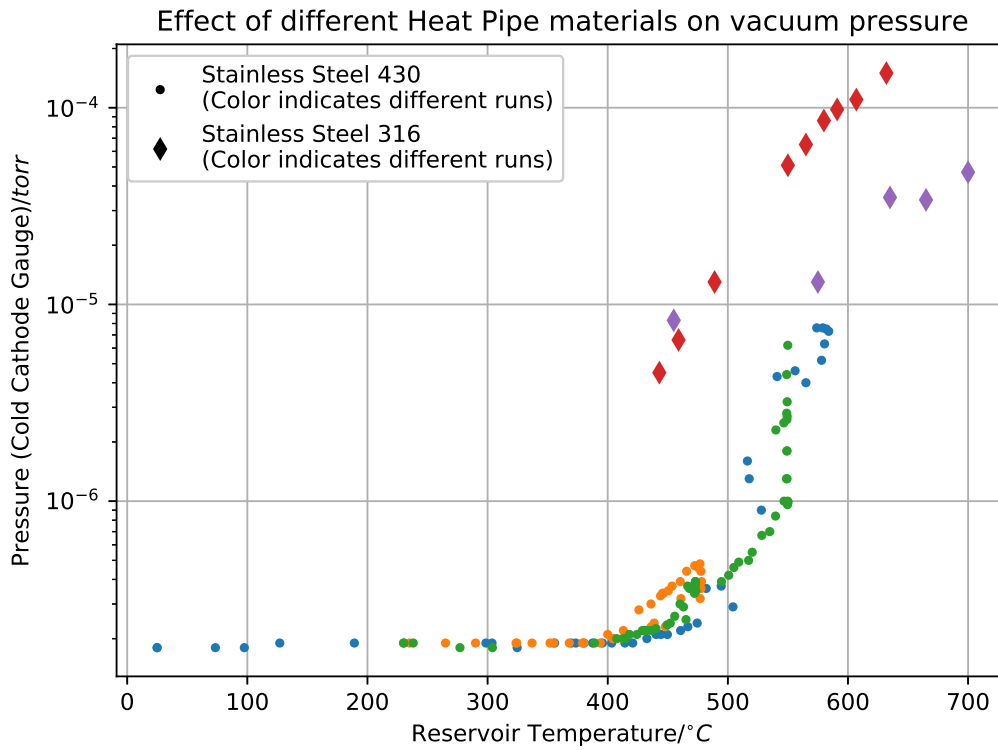


Figure 5.3: Pressure inside the heat pipe at different temperatures. The dots indicate measurements in a heat pipe made from stainless steel 430; diamonds indicate measurements made in a heat pipe consisting of stainless steel 316. The pressure levels in stainless steel 316 rise much higher than in 430 steel. This caused by the liquid lithium, which attacks the 316 steel so that hydrogen absorbed in the volume of the steel can desorbed. For stainless steel 430 the levels are lower since the steel is less corrosive under exposure to liquid lithium.

point, we probed the density of the lithium vapor using resonant absorption.

To this end the heat pipe was mounted in a vacuum system with viewports on both sides along the axis of the beam head, such that a laser beam could be passed through the heat pipe along its axis. We then measured the transmitted laser power as a function of the temperature of the reservoir at different heating powers. The results are shown in figure 5.4. As the temperature is increased from room temperature, the laser power drops as the vapor pressure of the lithium increases and the vapor becomes denser and more light is absorbed and isotropically reemitted.

At a temperature of approximately 500 °C however, this behavior changes and the transmitted laser power becomes basically flat at higher temperatures. This is because at this temperature, the lithium vapor in the beam head reaches a density at which the vapor becomes diffusive, i.e. it needs to be regarded as a collisional gas. At lower temperatures, the vapor is effusive, i.e. the mean free path of the individual lithium atoms is on the order of the size of the heat pipe and the vapor is largely collisionless.

When the lithium vapor becomes diffusive, its velocity distribution becomes broader and it expands inside the beam head towards the viewports. The expanding parts of the vapor have a large velocity component along the axis of the beam head and thus the propagation direction of the probing laser. The resonant frequency of the atoms is thus Doppler shifted away from the laser, which is tuned to atoms at rest. At some point, the Doppler shift becomes so large that the laser is off resonance with the fast atoms, which then

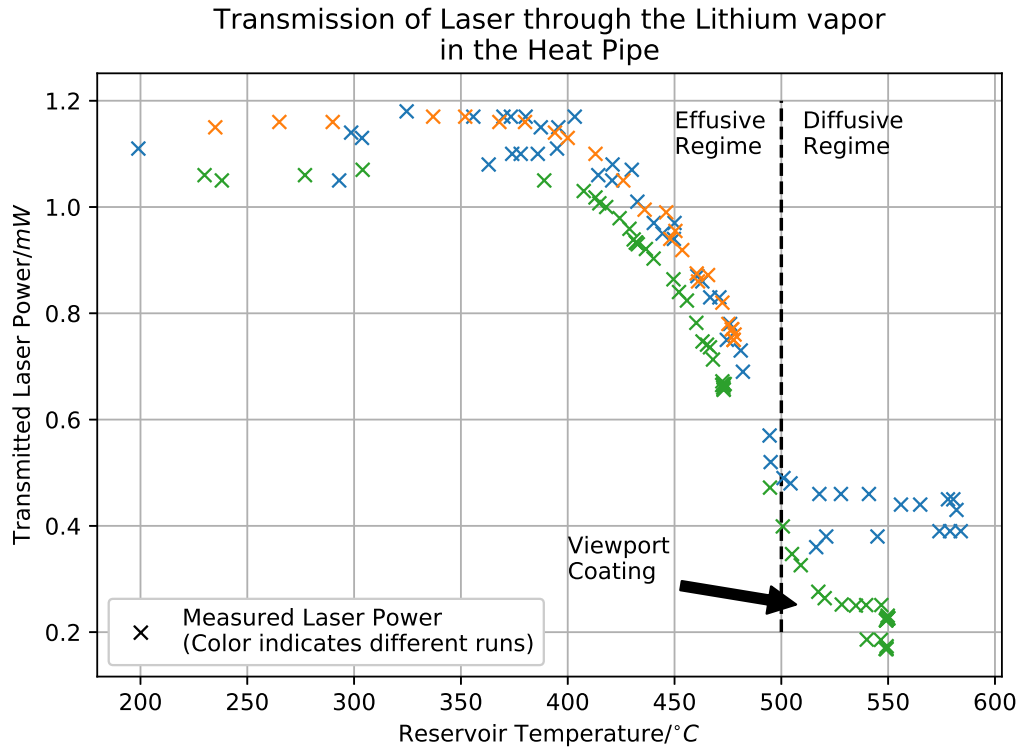


Figure 5.4: Transmitted laser power in an absorption measurement as a function of the reservoir temperature. The laser points along the axis of the heat pipe parallel to the propagation direction of the supersonic beam and passes over the opening of the reservoir. As the reservoir temperature increases, the laser power decreases, as the lithium vapor pressure increases and more lithium is emitted from the reservoir. At a temperature of 500 °C and higher, this behavior saturates. This is because at this point, the lithium cloud becomes collisional (diffusive regime) and starts to spread along the axis of the heat pipe. The lithium that spreads out can not be seen with this absorption measurement since it is Doppler-shifted off the laser frequency due to its velocity along the heat pipe axis and along the propagation direction of the laser. As the temperature increases further, the lithium reaches the viewports at the front and back end of the chamber through which the laser passes and starts coating them. This leads to a further decrease in the transmitted power, which does not regenerate when decreasing the temperature. To resume the experiment, the viewports need to be cleaned.

become undetectable. This leads to the change in behavior of the transmitted power in the diffusive regime as seen in figure 5.4.

At very high temperatures, the lithium vapor propagates far enough to coat the viewports through which the laser enters and exits the chamber. This means that after decreasing the temperature from temperatures in the diffusive regime, the transmitted beam power does not go back to its original value, but stays lower. This can be seen for the green data set in figure 5.4. For the power to reach the original values for low temperatures, the viewports need to be rinsed with water to remove the lithium off the glass surface and cleaned.

For entrainment, we want to operate at the boundary between the effusive and diffusive regime. The density of the lithium vapor should be high, so that a lot of atoms have a chance of being entrained into the supersonic helium beam. However, the lithium vapor density should not be too high as the supersonic helium beam would otherwise undergo excessive scattering off the lithium vapor which would increase its temperature.

To test entrainment, the heat pipe was mounted in between two large vacuum chambers. The first contained the supersonic nozzle and the skimmer and served to create the supersonic beam. The distance between the nozzle and the skimmer was 4".

Once past the skimmer, the supersonic beam propagated through the heat pipe beam head and passed over the reservoir at a distance of 8" from the

skimmer. After clearing the heat pipe, the beam entered another chamber that contained a Langmuir-Taylor detector at 25" from the nozzle and an RGA at 30". The Langmuir-Taylor detector measured the lithium flux as a function of time and the RGA measured the helium flux as a function of time.

A typical result is shown in figure 5.5. For this result, the supersonic nozzle was opened for 30 μ s at a stagnation pressure of 304 psi (2.10×10^6 Pa) and the reservoir was kept at a temperature of 530 °C. The figure shows the lithium and helium signals as a function of arrival time at the Langmuir-Taylor detector. The helium signal, which is measured 5" further downstream was shifted to account for the additional travel time, so that the timing between the two signals shown is as it would be, if the detectors were at the same position along the beam path.

The helium signal shows a large peak at 620 μ s superimposed on a much broader increasing background. At larger times than shown in the figure this background saturates and decreases. The narrow peak is generated by the arrival of the supersonic beam. The broad background is understood to be generated by helium that is scattered off axis and assumes a broad velocity distribution that is generally lower than the supersonic beam.

The lithium signal shows one single peak on a flat background. This peak however is much wider than the helium signal and it arrives about 300 μ s after the supersonic helium beam. This means, that both the mean velocity and the temperatures of the two beams are different, with the lithium being much slower and hotter, and thus the beams have not thermalized as intended.

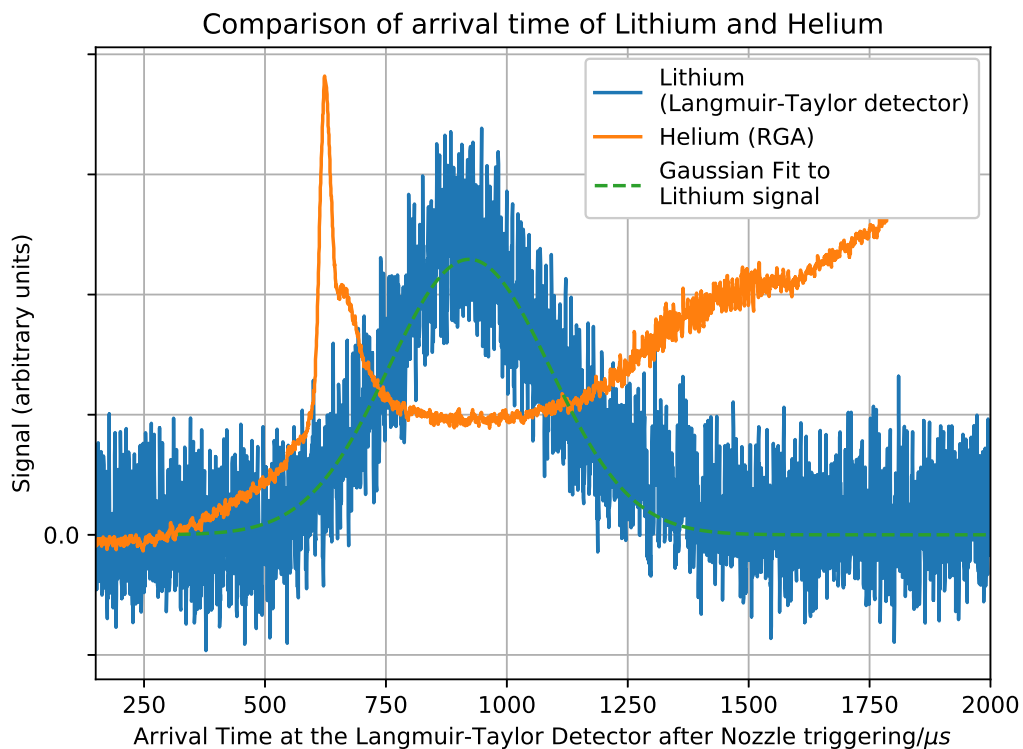


Figure 5.5: Sample plot showing the signal from the Langmuir Taylor detector measuring lithium and from the RGA measuring helium as a function of arrival time at the Langmuir Taylor detector. The RGA signal has been shifted in time to correct for a 5" difference in path length to the RGA. The supersonic nozzle was opened for $30 \mu\text{s}$ at a backing pressure of 304 psi (2.10×10^6 Pa) to create the shown helium beam. The reservoir of the heat pipe was at a temperature of 530°C . The amplitudes have been scaled to fit on the same axis. The helium beam arrives at the detector significantly earlier and it is much narrower than the lithium beam. This is a sign of failed entrainment, as there are not enough collisions between helium and lithium atoms to achieve equilibrium between the two species.

The fact that the mean velocity of the lithium beam is smaller suggests, that the flux of the helium beam in the heat pipe is too low. If the helium flux is too low, then a lithium atom would only undergo few collisions with atoms in the supersonic beam and thus not equilibrate. Since the initial mean velocity component of the lithium along the propagation direction of the supersonic beam is small, its mean velocity is smaller than the mean velocity of the helium beam.

The flux of the helium beam in the heat pipe is low because the heat pipe is at a large distance (12") from the supersonic nozzle and flux is decreased by the thermal spreading of the beam. Also, the beam loses flux when passing through the skimmer by one to two orders of magnitude [27]. It would thus be advantageous to move the heat pipe to a position before the skimmer, where the helium beam has much more flux. A design that does just that is presented in the following chapter.

Chapter 6

Heat Pipe Entrainment before the Skimmer

6.1 Design of a fixed Heat Pipe

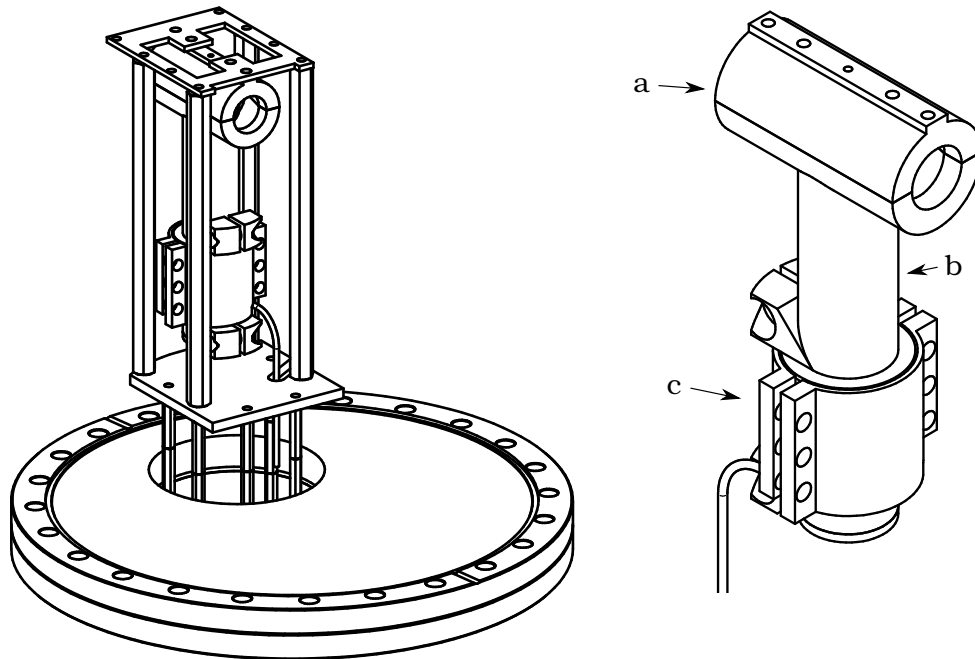


Figure 6.1: Schematic drawing of the "heat pipe" recirculation entrainment oven. The left side shows the heat pipe as it is mounted on a 10" conflat flange. On the right, the structure of the heat pipe is labeled as beam head (a), reservoir (b) and heater assembly (c).

Figure 6.1 shows a schematic drawing of the heat pipe recirculating entrainment oven that can be mounted between the supersonic nozzle and

the skimmer. The left side of the figure shows the heat pipe mounted on a 10" conflat flange. This flange attaches to the bottom flange of the vacuum chamber that houses both the supersonic nozzle on a cryo-cooled mount and the skimmer. In this design, the mount of the heat pipe is fixed, i.e. it cannot be translated in any direction by more than a few millimeters. This means that the its distance to the nozzle and thus the parameters of the supersonic beam that passes through the heat pipe cannot be changed by means of relocating the heat pipe.

The right side of figure 6.1 points out the different functional components of the heat pipe oven. These are the reservoir (b), which contains the lithium. The reservoir is heated by a heater assembly (c), which has the effect of raising the vapor pressure of the lithium to the point where individual lithium atoms leave the bulk liquid and spray upwards into the beam head (a). The beam head has openings for the supersonic beam to pass through and encloses it while it is passing over the opening of the reservoir. Thus, the beam head catches all lithium atoms that are not entrained. The captured lithium atoms can then be recirculated along the walls of the beam head into the reservoir.

In the following sections, I will discuss the design and function of the beam head, the reservoir, and the heater in greater detail.

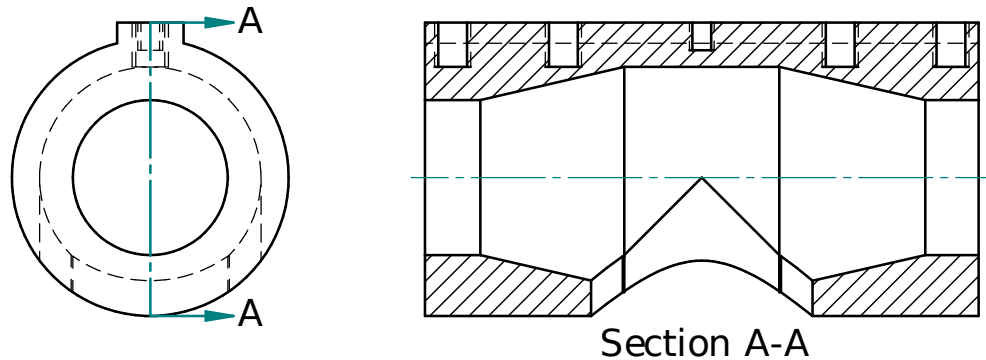


Figure 6.2: Cross section view of the heat pipe beam head along the propagation direction of the supersonic beam. The inlet and outlet openings for the supersonic beam have a diameter of 0.7", which is approximately 3.5 times larger than the diameter of the skimmer (5 mm). The inside surface of the beam head is angled to allow liquid lithium to flow back into the reservoir. The reservoir attaches to the large cutout at the bottom of the beam head, perpendicular to its axis.

6.1.1 Beam Head

A schematic of the beam head detached from the reservoir is shown in figure 6.2. It consists of a cylindrical shell with angled inside walls, such that the inner diameter is greatest in the center, where the reservoir attaches in the cutout at the bottom. The openings on the flat sides of the cylinder are large enough to accommodate the beam, with a diameter of 0.7" which is about 3.5 times the diameter of the skimmer of 5 mm. The openings are also small enough, such that there is no line of sight to the surface of the liquid lithium pool inside the reservoir. This is important to assure that lithium atoms that desorb from the bulk liquid cannot find a direct path leaving the heat pipe, as such atoms could not be recirculated. Instead, all lithium atoms that do not entrain into the supersonic beam will hit the wall of the beam head and they

will stick to that wall.

To achieve recirculation of the lithium that attaches to the beam head walls, the surface needs to be at a high enough temperature for the lithium not to solidify. However, it also needs to be cold enough such that the vapor pressure of the lithium on the walls is sufficiently small such that reemission of lithium from the walls is small. Reemission is undesired as direct paths leaving the heat pipe are accessible from all points on the inner surface of the beam head and loss of some fraction of the reemitted lithium can not be avoided. A plot of the vapor pressure is shown in figure 3.2.

6.1.2 Reservoir

The reservoir consists of a hollow cylindrical tube that is mounted perpendicularly onto the head head. The purpose of the reservoir is to contain the lithium at a variety of temperatures.

The reservoir has an inner diameter of 0.9" and an outer diameter of 1.0". It measures 4.625" from the center of the beam head to its bottom end. These dimensions are chosen such that the pool of liquid lithium that will form in the bottom of the reservoir tube will not have a line of sight to the circular openings of the beam head. In particular, if the surface of liquid lithium is one inch above the bottom of the reservoir, the conical beam exiting the reservoir into the beam head will have an opening half-angle of less than 20°. In this case, all the emitted lithium will hit the beam head surface, which is kept hot enough so that the lithium can flow back into the reservoir.

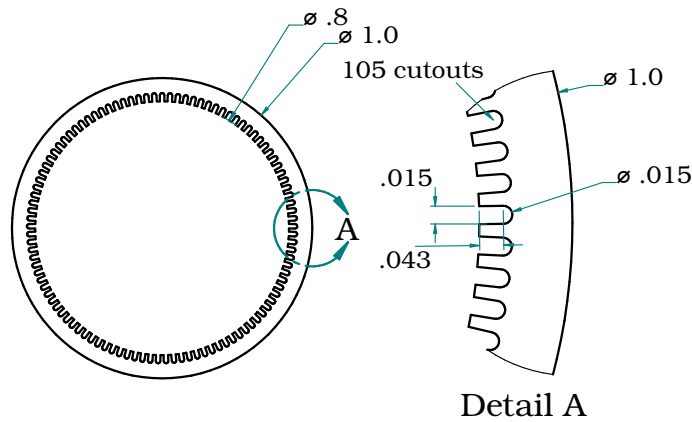


Figure 6.3: Cross-section through the reservoir perpendicular to its cylindrical axis. Visible are the small cylindrical cutouts on the inside wall that wick liquid lithium back into the reservoir through capillary action. All labeled values are in units of inches.

To enhance the flow of lithium back into the reservoir, the walls of the reservoir are fitted with 105 small grooves that are 0.015” in diameter and 0.05” deep (see figure 6.3). These grooves have been cut in the local machine shop using a electric discharge machine [48]. As the liquid lithium fills these grooves, it wets the walls and thus experiences pressure due to capillary action. This pressure is given by $P = 2\frac{\sigma}{r}$ [44], where $\sigma = 0.386 \text{ N/m}$ [58] is the surface tension of liquid lithium at the considered temperatures and r is the radius of curvature in the grooves. The pressure due to capillary action is then $4 \times 10^3 \text{ Pa}$ or 30 torr. The effect of capillary action in recirculating the liquid lithium is significant.

Experimentally, it was also visually observed after removing the heat pipe oven from the vacuum system that the grooves are filled with resolidified lithium, confirming that the grooves do collect the lithium through capillary

action.

6.1.3 Heater Assembly

The lithium reservoir is heated with an electrical heater wrapped in a copper assembly at the foot of the reservoir.

The heater assembly is a compact cylindrical shell of 1.6” OD and 1” ID. It is 1.5” tall along the cylinder axis. The total wall thickness of the heater is 0.3”. This small dimension contains an inner copper sheet with groves for the heater wire, the actual heater wire, and an outer copper sheet, which clamps the heater wire to the inner copper shield.

The choice of copper as a material is mostly due to its excellent heat conduction. However, it raises the question of different thermal expansion between the shaft that the heater will clamp to, which is 430 stainless steel, and the heater. The coefficient of thermal expansion for 430 steel is approximately $12 \times 10^{-6} / \text{K}$ [66] and $16.5 \times 10^{-6} / \text{K}$ for copper [37]. Considering the diameter of 1” of the cylindrical steel-copper interface and a temperature change of 600 K, this would yield a difference in expansion of less than 0.004” in the diameter, which is acceptable. Since the alignment between the cylinder axes of heater and shaft will not be perfect due to torque from the heater wire connection and since the material surfaces will not be perfectly smooth, it is very unlikely that the heater will fall off the shaft when heated.

The inner sheet of copper has a solid thickness of 0.1”. On the outside of this sheet, there are groves that accommodate an ohmic heater wire of

0.093" diameter. The groves extend to slightly more than half of the heater wire radius out of the sheet bulk.

The inner sheet is one single part, but there is a cut parallel to the cylinder axis that allows for slight compression of the diameter to facilitate clamping of the heater to the shaft. Two screws that fit into the extended screw-holes at top and bottom of the inner sheet clamp the heater to the shaft.

The heater wire that is used is a industrial heater assembly manufactured by Ari Industries. It consists of a resistive nickel-chrome iron core that is wrapped in an Inconel sheet with an insulation of ceramic dust. The heater wire is flexible enough to be coiled around the copper heater assembly. It has a hot length of 38" and a cold length of 4", where the resistive core is replace with a less resistive material. To accommodate the hot length on a spool with a diameter of approximately 1.3", 9.5 revolutions are required. This can be easily accommodated by winding the 0.093" diameter heater wire with a center-to-center pitch of 0.13", which requires groves over a length of 1.3" along the surface of the inner shell.

The outer sheet consists of two parts, each shaped as a cylinder shell cut in half along the cylinder axis. These two symmetric parts clamp the heater wire from the outside, holding it in place in the groves on the inner sheet.

6.1.4 Comparison of Expected Flux to the Capillary Oven

The design goal of the heat pipe oven is to entrain more atoms into the supersonic beam than the capillary oven. To this end, the design flux of lithium atoms out of the heat pipe reservoir is larger than the flux out of the capillary oven.

The flux Q of a molecular beam emerging from a heated cavity with open surface A is given by the following equation [67]:

$$\begin{aligned} dQ &= \frac{1}{4\pi} n \bar{v} \cos(\theta') A d\omega \\ \Rightarrow Q &= \int_0^{2\pi} \int_0^\theta \frac{1}{4\pi} n \bar{v} \cos(\theta') \sin(\phi) d\theta' d\phi \\ &= \frac{1}{2\pi} n \bar{v} A \sin \theta \end{aligned} \quad (6.1)$$

where n is the number density inside the cavity, \bar{v} is the mean velocity of particles inside the cavity and θ is the half-angle of the exiting beam-cone.

The opening of the capillary oven is an equilateral triangle with the length of one side being 0.603". It is filled with capillary tubes of inner diameter 0.0355" and length of 0.9". It is kept at a temperature of 900 K.

The opening half-angle that is allowed for by the capillaries is thus:

$$\theta = \arctan\left(\frac{.0355}{2 \cdot .9}\right) \approx .019 \approx 1.1^\circ \quad (6.2)$$

and the open area through which the beam escapes is (assuming infinitely thin capillary walls):

$$A_O = s \cdot \sqrt{s^2 - \frac{s^2}{4}} = \sqrt{\frac{3}{4}} s^2 \approx 2.03 \cdot 10^{-4} m^2 \quad (6.3)$$

The heat pipe is kept at a temperature of 800 K, which is lower than the temperature of the oven in order to conserve lithium. The effective opening half-angle of the lithium beam emerging from the heat pipe reservoir into the beam-head is at least 10° , during normal operation, with a higher filling level, it will be larger. This is wider than for the capillary oven as the beam angle is only restricted by the walls of the reservoir of diameter 0.9". The area of the opening is thus $4.1 \times 10^{-4} \text{ m}^2$, respectively.

From these values and equation 6.1, the flux out of the heat pipe Q_{HP} is higher than that from the Oven Q_O by the following factor:

$$\frac{Q_{HP}}{Q_O} = \frac{\bar{v}_{HP} A_{HP} \sin(\theta_{HP})}{\bar{v}_O A_O \sin(\theta_O)} = \frac{\sqrt{T_{HP}} A_{HP} \sin(\theta_{HP})}{\sqrt{T_O} A_O \sin(\theta_O)} \quad (6.4)$$

This expression evaluates to 17 for the heat pipe with the given reservoir diameter.

The flux from the heat pipe is thus considerably larger than the flux from the capillary oven.

6.2 Thermal Behavior

An important design goal in constructing the heat pipe is meeting different temperature requirements in the beam head and in the reservoir. The temperature in the reservoir should be high to achieve a high lithium vapor pressure and thus high flux. It should not be too high however, so that the lithium vapor is still largely atomic. The temperature targeted in the design is between 500°C and 600°C . The temperature in the beam head however

needs to be much lower, to minimize the vapor pressure and suppress lithium reemission, while keeping the lithium liquid for recirculation. The targeted temperature here is 200 °C to 300 °C, just above the melting point of lithium [37].

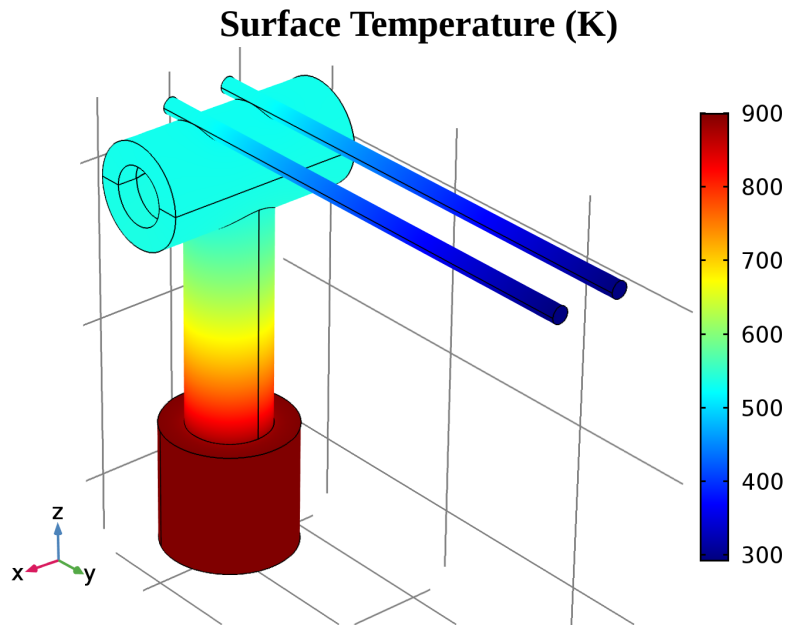


Figure 6.4: Temperature profile of the heat pipe when reservoir is held at 900 K. This simulation shows how the temperature drops from the bottom of the reservoir to the beam head. For ideal operation, the reservoir should be hot to generate a large vapor pressure of the liquid lithium, whereas the top part of the reservoir and the beam head stay at cooler temperatures of around 500 K to avoid secondary emission of accumulated lithium atoms. The temperature in the top is however still hot enough for the lithium not to solidify so that it can be recirculated into the reservoir.

To satisfy these requirements, I performed finite element simulations of the temperature distribution in candidate designs using *Comsol Multiphysics*. The result of one such simulation is illustrated in figure 6.4. This simulation

considered a heat pipe design that is identical to the one presented above except for the mounting structure. The mounting of the simulated heat pipe is through two cylindrical rods whose combined cross section is comparable to the narrowest cross section in the holding plate that the final design used for mounting (see figure 6.1).

The end of the rods in the simulation is held fixed at room temperature to simulate heat loss through the mounting structure to the vacuum chamber. Thermal coupling to the chamber is in fact intended to cool the beam head and achieve and maintain a temperature gradient from the bottom of the reservoir to the top. The reservoir heater assembly is approximated by a copper cylindrical shell whose outside mantle is kept at a fixed temperature of 900 K. The simulation further considers radiative heat loss to a radiation environment at room temperature.

The results of the simulation show the development of a temperature gradient across the upper portion of the reservoir which is not directly covered by the heater. The beam head, with greater wall thickness and larger thermal mass is at a roughly constant temperature of 540 K throughout its volume. This temperature is suitable to keep the lithium from solidifying, while maintaining a low vapor pressure.

To achieve this temperature distribution, several different designs with varying wall thickness in the upper part of the reservoir have been simulated to find a wall thickness that would allow for the right amount of heat flux to the beam head to achieve a suitable temperature. The wall thickness in the

shown simulation is 0.1", which does not consider the height of the capillary grooves.

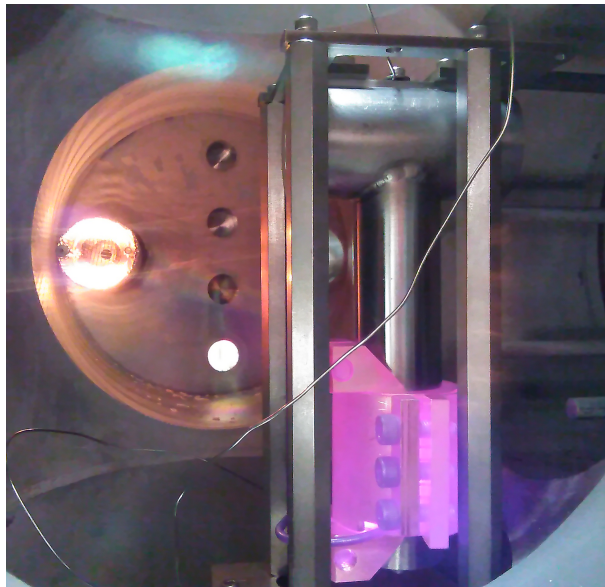


Figure 6.5: View of the assembled heat pipe in the vacuum system during baking. The copper heater assembly is heated to 600°C and visibly glows. The camera is sensitive to the near infrared which is rendered as violet, which is responsible for the coloring of the glowing copper. In the background, the incandescent filament of the residual gas analyzer is visible. The steel-plated wires in the foreground are thermocouples used to measure the temperature at the top of the beam head and at the bottom of the reservoir, below the heater assembly. The bright spot near the lower edge of the flange in the background is a viewport illuminated from behind.

After assembly, the temperature predictions were tested by baking the heat pipe in a separate chamber prior to loading it with lithium. The temperature was measured by two thermocouple wires, one situated at the top of the beam head, the other on the bottom surface of the reservoir. The heater has been supplied with a DC power supply.

A photographical picture of this setup is shown in figure 6.5. At the time of the photograph, the heater assembly was at a temperature of 600 °C. At this temperature the copper glows orange-red. Due to the partial sensitivity of the camera to near infrared, the color in the picture is distorted to violet.

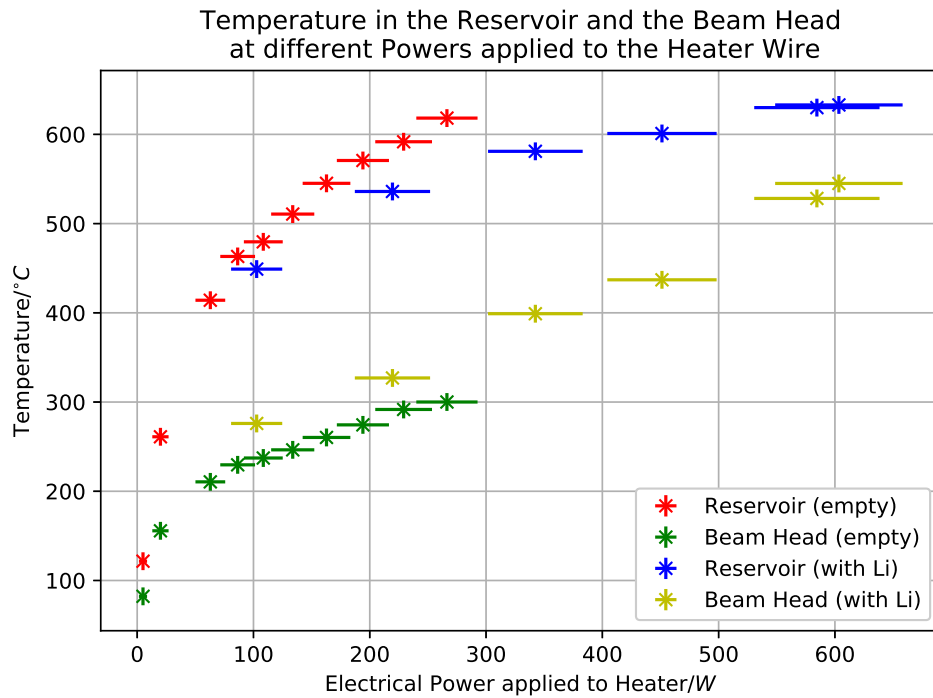


Figure 6.6: Temperature at the top of the beam head and at the bottom of the reservoir at different applied electrical heating powers.

The temperatures that have been recorded in this way without lithium are shown in figure 6.6 as a function of the electrical power that was applied to the heater. This figure also shows temperature data that was taken during the operation of the heat pipe for entrainment loaded with lithium. Without lithium, the temperatures of the beam head and the reservoir increase with

the applied power and their temperatures diverge, with the temperature in the reservoir always being about twice the temperature in the beam head. The temperatures that are achieved in this way are suitable for our application.

The temperatures that have been measured when the heat pipe was loaded with lithium show a slightly different behavior. The reservoir temperature with lithium is always lower than without lithium, while the reverse case is true for the beam head, which is always hotter with lithium than without. Besides that, at low applied powers of 100 W to 200 W, they follow the behavior of the temperatures of the unloaded heat pipe and diverge. However, at higher powers, the difference between the two temperatures becomes smaller.

There are several effects that are responsible for the differences in thermal behavior of the loaded and unloaded heat pipe. First, as the lithium melts, the capillary grooves fill with liquid lithium. This increases the cross-sectional area of the path of thermal conduction between the reservoir and the beam the. The thermal power P that flows from the reservoir to the beam head due to conduction depends on this cross section A in the following way [68]:

$$P = -A \cdot \lambda \cdot \frac{\partial T}{\partial z} \quad (6.5)$$

This equation assumes $\frac{\partial T}{\partial z}$ to be the temperature gradient along the axis of the reservoir that is independent of the radial and azimuthal directions and only depends on the coordinate along the axis of the reservoir. Further, λ is the coefficient of thermal conduction. The power transferred from the reservoir to the beam head thus scales linearly with the cross-sectional area of the reservoir

walls and the attached lithium.

Second, another mechanism is needed to explain why the temperature difference between the reservoir and the beam head drops at high applied powers and high temperatures. If the temperature difference is small, then conducted power decreases as $\propto \frac{\partial T}{\partial z}$. A smaller temperature difference is thus not achievable only through conduction. This decrease in temperature difference suggests, that the heat pipe is in fact actually working as a heat pipe! A heat pipe is a device, that transports heat through the evaporation of medium at a hot surface and condensation at a cold surface and subsequent recirculation [46]. And in fact this is what happens in our heat pipe as well: At high temperatures, the lithium reaches high vapor pressures, is emitted and travels in a molecular beam to the beam head, where it condenses, thus depositing heat that it transported away from the reservoir.

This effect was unfortunately not considered in the design of the heat pipe, which led to the beam head temperature during all experiments being larger than predicted and thus lithium was able to escape through the openings of the beam head into the bulk of the vacuum chamber.

For a future design, it would be advantageous, to have independent control over the temperatures of the beam head and the reservoir and not to rely on designed geometry only, as multiple, temperature dependent mechanisms of heat transport are at work.

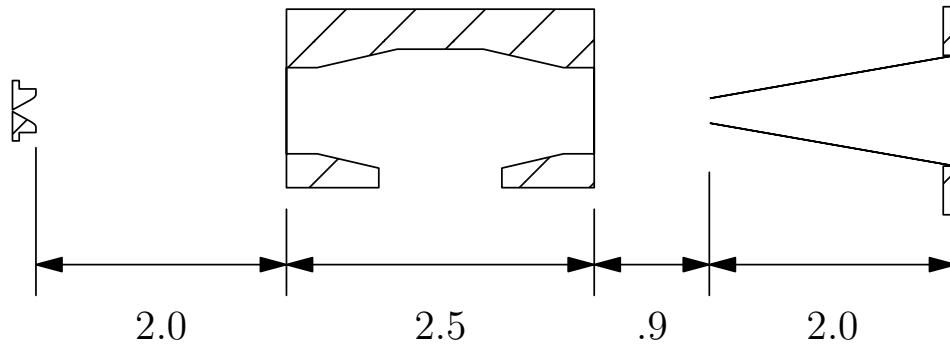


Figure 6.7: Schematic of the spacial positions of the heat pipe beam head, the supersonic nozzle, and the skimmer, relative to each other. All values are in units of inch.

6.3 Interaction with the Helium Beam and Entrainment

To test entrainment with this heat pipe, it was placed in between the supersonic nozzle and the skimmer. The distance to the nozzle is 2.0" and the distance to the skimmer was 0.9" as sketched in figure 6.7. This places the heat pipe in the middle of the flow field of the supersonic nozzle, with a much higher flux of helium which would suggest more interaction between the helium and the lithium, but also between the helium beam and the geometry of the heat pipe. This section summarizes the observed effects.

Several experiments have been performed to characterize the helium beam and the lithium beam obtained from this setup behind the skimmer. To measure the lithium and helium signals as a function of time-of-flight, an RGA has been used that was mounted on a 2.75" conflat cross such that the center of the incandescent filament is on the axis of propagation of the beam, approximately 4.5" behind the opening of the skimmer. The RGA

was mounted perpendicular to the propagation direction of the beam. Due to spatial constraints so close behind the skimmer, the Langmuir-Taylor detector was not used to measure the lithium, instead the charge-to-mass ratio of the RGA was tuned to lithium and the RGA was used to probe the lithium flux. In this configuration, helium and lithium flux cannot be measured simultaneously. Instead, lithium and helium signals were obtained in successive nozzle pulses.

The transmission of the helium beam through the heat pipe and the skimmer were also measured with the heat pipe at room temperature to be able to distinguish effects that are solely due to the heat pipe geometry from effects due to interaction with the lithium.

Experimental results are shown in figure 6.8. Measurements have been performed at different nozzle stagnation pressures of $P = 50$ psi (3.4×10^5 Pa), $P = 100$ psi (6.9×10^5 Pa), $P = 200$ psi (1.4×10^6 Pa), and $P = 500$ psi (3.4×10^6 Pa). These different backing pressures correspond to the four rows in figure 6.8 from top to bottom. For each backing pressure, the helium flux with the heat pipe at room temperature, as well as the helium flux and the lithium flux with the reservoir at a elevated temperature have been measured as a function of time-of-flight for different nozzle pulse lengths. The temperatures of the reservoir and the beam head during these experiments varied in the ranges of (550 ± 40) °C and (400 ± 40) °C, respectively. These groups of measurements have been visualized as color-maps, with the color indicating flux in arbitrary units, the vertical axis denoting the arrival time at the sensor, and the horizontal axis denoting the pulse length of the supersonic nozzle. To

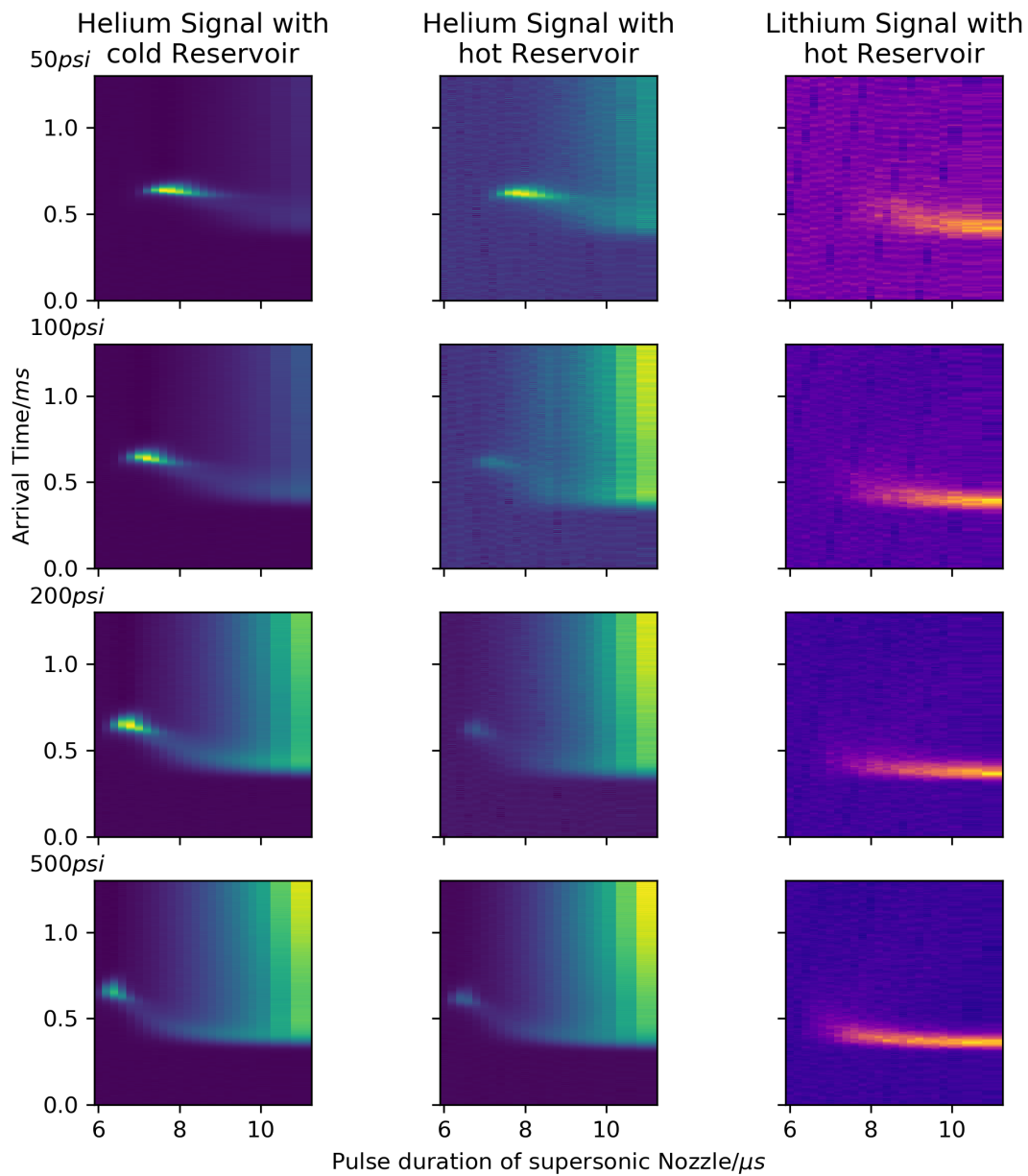


Figure 6.8: RGA measurements of the helium beam and the lithium from the experimental pipe after the skimmer.

make the qualitative behavior of the beams in the different situations more readily apparent, the color scales for all the plots are different for the different plots. Otherwise, features in the individual plots would be barely noticeable.

The helium flux signals in figure 6.8 all share some basic similarity. In all of them, there is a peak at lower pulse lengths, that arrives at approximately $700 \mu\text{s}$ and is approximately $50 \mu\text{s}$ long. At large pulse lengths, there is a frontal peak at $400 \mu\text{s}$ that is followed by a long rising tail that eventually decays back to a zero level long after first arrival (not shown). The boundary between these two regimes is at shorter pulse lengths for higher backing pressure. In the boundary region, the flux is low and the arrival time of its maximum moves to earlier times with increasing pulse duration. For all backing pressures, the flux in the long tail at long pulse lengths is larger with respect to the frontal peak and the peak at low pulse lengths for the case of a heated reservoir.

The peak at low pulse lengths can be identified with a (relatively) undisturbed supersonic beam. At higher stagnation pressures, it moves to earlier pulse lengths, as the nozzle actuation becomes more reactive. However at pulse lengths shorter than $6 \mu\text{s}$ we never observe a pulse as the nozzle does not open for such short pulses. At longer pulse lengths, the supersonic beam disappears and a different flow regime becomes dominant due to scattering off the heat pipe geometry. The supersonic beam can form at low pulse lengths as scattering is not as important as for longer pulse lengths. First, this is due to the lower total atom number in the helium beam at lower pulse lengths, which causes the mean free path inside the beam to become longer so that scattered

atoms disturb the rest of the beam less. Second, the short pulse length means that disturbances in the beam have less time to propagate from the point of their origination to other regions of the beam before the beam has moved past the region of disturbance.

At long pulse lengths, many more atoms flow down the beam line and continuous effects play a more important role. On the front face of the beam head, the flow outside of the central axis is decelerated due to collisions with the beam head and the pressure increases locally, which leads to shocks that propagate into the unscattered flow close to the axis of the beam head and disturb the supersonic beam. The higher densities inside the beam head cause the beam to behave more like the molecular flow in a duct rather than free molecular flow. This provides a mechanism that can influence the velocity of the beam [28], and cause the acceleration and thus the arrival of a frontal peak at earlier times in figure 6.8. However, a significant part of the beam is strongly disturbed, no longer supersonic, and with a broad velocity distribution, which causes the long tail.

At transition from the regime of the weakly disturbed supersonic beam at short pulse lengths to the strongly disturbed flow at large pulse lengths, the supersonic beam gradually loses flux until it disappears. In parallel, a second, smaller and broader peak forms which is influenced by the interactions with the beam head geometry and accelerates to arrive at earlier times at longer pulse lengths. At even higher pulse lengths, the long tail forms due to increased scattering, which in turn is due to a higher number of helium atoms

in the beam. At higher pulse lengths, a larger and larger fraction of the beam transitions into the tail, until the tail and the frontal peak are indiscernible.

At higher stagnation pressures, the transition between the two regimes moves to shorter pulse lengths. This is due to the beam having a higher flux at higher backing pressures and thus continuous effects start to be important at shorter pulse lengths.

The long tail is generally more important in the presence of the lithium vapor. The explanation for this is just that the lithium atoms constitute additional scattering targets that disturb the flow.

The lithium signal curiously only exists in the regime of long pulse lengths, no lithium was detected in the weakly disturbed supersonic beam. The explanation for this absence is that in the regime of the supersonic beam, the mean free path of the lithium inside the helium beam is so long that it does not get entrained.

Lithium has however been observed at long pulselengths, at arrival times just early of the arrival of the frontal peak in the helium signal. The long tail does however not contain any lithium at all. The lithium peak becomes narrower at higher stagnation pressures, however, it is always hotter than the frontal peak in the helium signal. An explanation for this would be that the helium beam in this regime is so dense, that all the lithium is pushed along by the frontal peak that forms through continuous acceleration in the beam head. The velocity distribution of this peak is however much wider than for

the supersonic beam and thus corresponds to larger beam temperatures. The lithium is however not properly entrained, as its arrival time and temperature do not match the helium beam.

To summarize, the heat pipe interacts in a complex manner with the helium beam, changing its properties dramatically. Only at very low pulse length, too low for entrainment, can this interaction be avoided and a supersonic beam be maintained. At longer pulse lengths, the helium beam divides into a frontal peak that is faster and broader than the supersonic beam and is able to entrain lithium, and a long tail of heavily scattered lithium gas with very wide velocity distribution.

To successfully entrain using a heat pipe before the skimmer, the interaction with the supersonic flow must be minimized. We expect, that this should be possible by changing the position of the heat pipe. The density of the flow decreases with distance from the nozzle. Thus the disturbance of the supersonic beam should be smaller when moving the heat pipe closer to the skimmer. Another approach to suppress the forming of a continuous flow inside the beam head would be to increase its diameter.

Chapter 7

Conclusion

Two different approaches to entraining lithium into a supersonic helium beam using a recirculating heat pipe oven have been investigated: Entrainment behind the skimmer and entrainment before the skimmer.

Behind the skimmer, the lithium does not thermalize with the helium beam and instead keeps a lower mean velocity and a much broader velocity distribution. It thus does not interact enough with the supersonic beam to assume its properties. The reason for this is that the density of the supersonic beam is too low to enable the number of collisions that is required for entrainment.

Before the skimmer there is significant interaction between the geometry of the heat pipe and the helium beam, which destroys the supersonic beam and creates a broader faster frontal peak followed by a long tail. Lithium is entrained into the frontal peak, however, it does not have the desired properties of the supersonic beam like low temperature in the moving frame.

Due to the evolution of the supersonic beam before the skimmer the second approach seems more promising, as different flow regimes can be explored by simply changing the geometry by e.g. translation of the heat pipe

downstream towards the skimmer or widening the beam head.

Chapter 8

Future Work

Based on the experience with the heat pipe ovens in this work, a new design has been composed. This new heat pipe is again meant for operation before the skimmer. It addresses the following shortcomings of the previous design:

- Fixed geometry with respect to the distance to the nozzle and the skimmer
- Insufficient temperature control of the beam head and overheating

The following two sections describe these design changes in greater detail.

8.1 Linear Translation along the Beam Path

To explore the behavior of the interactions between the helium beam and the geometry of the heat pipe, a simple linear translation system has been devised that can be added to the current setup with minimal effort. A schematic drawing is shown in figure 8.1. It consists of a redesign of the mounting structure of the heat pipe. The four large standoffs have been moved further apart to give ample space in between to freely position the heat pipe.

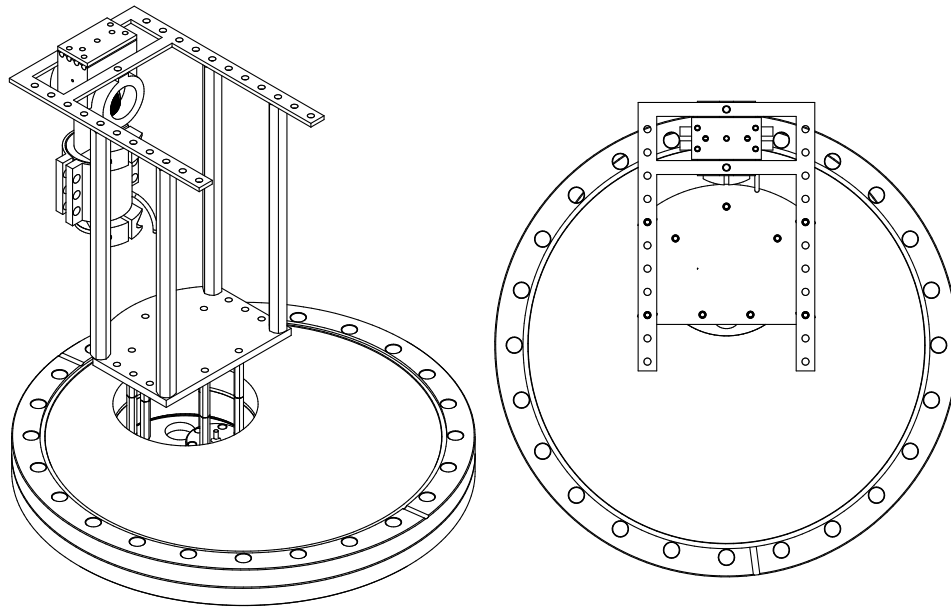


Figure 8.1: Conceptual drawing of the heat pipe oven with a translation stage (left: corner view, right: top view). The heat pipe is held at the top by a stainless steel plate that can be mounted to the holding structure with different offsets in steps of 0.5" by moving the hole pattern along one step. There is a copper block on top of the beam head that serves as a heat sink and is fitted with grooves at the top, that house tubing with flowing air or water (tubing not shown) to actively cool the beam head.

The heat pipe is mounted on a plate that is screwed to the top of the standoffs. The pattern of clearance holes for the screws is repeated several times with offsets of 0.5", immediately allowing for positioning of the heat pipe with this precision. Should finer adjustment of the position become desirable, new holes can be added easily. This system would allow for easy repositioning of the heat pipe anywhere between the nozzle and the skimmer.

8.2 Active Cooling System

Better temperature control of the beam head can be achieved using an active cooling system. This system consists of a copper heat sink that fits on top of the beam head (see figure 8.1). The top part of the heat sink features four grooves that house snaked copper tubing. The tubing is fixed by a copper clamp. A photograph of this assembly is shown in figure 8.2. The tubing connects to feedthroughs so that air or fluid can be run through the tubing to transport heat away from the beam head. Control of the temperature can be achieved by controlling the flow rate of coolant through the tubing.



Figure 8.2: Image of the cooling assembly that mounts on top of the beam head. The copper tubing runs across the top of the heat sink four times and it is recessed into grooves for better thermal coupling. The heat sink approximates the shape of the beam head and fits tightly. There is one hole in the side face of the heat sink that allows for mounting of a thermocouple wire to measure the temperature of the top of the beam head, underneath the heat sink.

Bibliography

- [1] K. B. Davis, M.-O. Mewes, M. R. Andrews, N. J. van Druten, D. S. Durfee, D. M. Kurn, and W. Ketterle. Bose-einstein condensation in a gas of sodium atoms. *Physical Review Letters*, 75(22), November 1995.
- [2] M. H. Anderson, J. R. Ensher, M. R. Matthews, C. E. Wieman, and Cornell E. A. Observation of bose-einstein condensation in a dilute atomic vapor. *Science*, 269(5221):198–201, July 1995.
- [3] Marios C. Tsatsos, Jason H. Nguyen, Axel U. J. Lode, Gustavo D. Telles, Vanderlei S. Bagnato, and Randall G. Hulet. Granulation in an atomic bose-einstein condensate, 2017. arXiv:1707.04055.
- [4] Pedro E. S. Tavares, Amilson R. Fritsch, Gustavo D. Telles, Mahir S. Hussein, François Impens, Robin Kaiser, and Vanderlei S. Bagnato. Matter wave speckle observed in an out-of-equilibrium quantum fluid. *Proceedings of the National Academy of Sciences*, 2017.
- [5] R. H. Chaviguri, T. Comparin, V. S. Bagnato, and M. A. Caracanhas. Phase transition of ultracold atoms immersed in a bose-einstein-condensate vortex lattice. *Physical Review A*, 95(053639), May 2017.
- [6] G. Rosi, F. Sorrentino, L. Cacciapuoti, M. Prevedelli, and G. M. Tino.

Precision measurement of the newtonian gravitational constant using cold atoms. *Nature*, 510:518–521, June 2014.

- [7] Andreas Wicht, Joel M. Hensley, Edina Sarjlic, and Steven Chu. *Condensation and Coherence in Condensed Matter*, chapter A Preliminary Measurement of the Fine Structure Constant Based on Atom Interferometry, pages 82–88. Physica Scripta and The Royal Swedish Academy of Sciences, 2011.
- [8] Savas Dimopoulos, Peter W. Graham, Jason M. Hogan, Mark A. Kasevich, and Surjeet Rajendran. Gravitational wave detection with atom interferometry. *Physics Letters B*, 678:37–40, 2009.
- [9] Klaus Blaum, Mark G. Raizen, and Wolfgang Quint. An experimental test of the weak equivalence principle for antihydrogen at the future FLAIR facility. *International Journal of Modern Physics: Conference Series*, 30(1460264), 2014.
- [10] M. Jerkins, J. R. Klein, J. H. Majors, F. Robicheaux, and M. G. Raizen. Using cold atoms to measure neutrino mass. *New Journal of Physics*, 12(043022), 2010.
- [11] M.-O. Mewes, M. R. Andrews, D. M. Kurn, D. S. Durfee, C. G. Townsend, and W. Ketterle. Output coupler for bose-einstein condensed atoms. *Physical Review Letters*, 78(4):582–585, January 1997.

- [12] Jamie R. Gardner, Erik M. Anciaux, and Mark G. Raizen. Communication: Neutral atom imaging using a pulsed electromagnetic lens. *Journal of Chemical Physics*, 146(081102), 2017.
- [13] Rodrigo Castillo-Garza, Jamie Gardner, Sagi Zisman, and Mark G. Raizen. Nanoscale imaging of neutral atoms with a pulsed magnetic lens. *ACS Nano*, 7(5):4378–4383, 2013.
- [14] William D. Phillips. Nobel lecture: Laser cooling and trapping of neutral atoms. *Reviews of Modern Physics*, 70(721), July 1998.
- [15] I. D. Setija, H. G. C. Werij, O. J. Luiten, M. W. Reynolds, T. W. Hijmans, and J. T. M. Walraven. Optical cooling of atomic hydrogen in a magnetic trap. *Physical Review Letters*, 70(2257), 1993.
- [16] E. S. Shuman, J. F. Barry, and D. DeMille. Laser cooling of a diatomic molecule. *Nature*, 467:820–823, October 2010.
- [17] Marcia J. Isakson and Greg O. Sitz. Adsorption and desorption of HCl on ice. *Journal of Physical Chemistry*, 103:2044–2049, January 1999.
- [18] Leah C. Shackman and Greg O. Sitz. State-to-state scattering of D_2 from Cu(100) and Pd(111). *Journal of Chemical Physics*, 123(064712), 2005.
- [19] Adam Alexander Libson. *General Methods of Controlling Atomic Motion: Experiments with Supersonic Beams as a Source of Cold Atoms*. PhD thesis, The University of Texas at Austin, December 2012.

- [20] Adam Libson, Stephen Travis Bannerman, Robert J. Clark, Thomas R. Mazur, and Mark G. Raizen. The atomic coilgun and single-photon cooling. *Hyperfine Interactions*, 212:203–212, December 2012.
- [21] Etay Lavert. *Control of mean velocities of supersonic beams*. PhD thesis, Weizmann Institute of Science, 2014.
- [22] Yuval Shagam, Ayelet Klein, Wojciech Skomorowski, Renjie Yun, Vitali Averbukh, Christiane P. Koch, and Edvardas Narevicius. Molecular hydrogen interacts more strongly when rotationally excited at low temperatures leading to faster reactions. *Nature Chemistry*, 7:921–926, November 2015.
- [23] Nitzan Akerman, Michael Karpov, Yair Segev, Natan Bibelnik, Julia Narevicius, and Edvardas Narevicius. Trapping of molecular oxygen together with lithium atoms. *Physical Review Letters*, 119(073204), 2017.
- [24] Mark G. Raizen, Dmitry Budker, Simon M. Rochester, Julia Narevicius, and Edvardas Narevicius. Magneto-optical cooling of atoms. *Optics Letters*, 39(15), August 2014.
- [25] Karl A. Burkhardt. A comparative study of entrainment in supersonic beams. Master’s thesis, The University of Texas at Austin, August 2016.
- [26] Uzi Even. The even-lavie valve as a source for high intensity supersonic beam. *EPJ Techniques and Instrumentation*, 2(17), 2015.

- [27] Uzi Even. Pulsed supersonic beams from high pressure source: Simulation results and experimental measurements. *Advances in Chemistry*, Article ID 636042, August 2014.
- [28] Giovanni Sanna and Guiseppe Tomassetti. *Introduction to Molecular Beams Gas Dynamics*. Imperial College Press, 2005.
- [29] Hans Pauly. *Atom, Molecule, and Cluster Beams 1: Basic Theory, Production and Detection of Thermal energy Beams*. Springer Series on Atomic, Optical, and Plasma Physics. Springer, 2000.
- [30] G. A. Bird. *Molecular Gas Dynamics*. Clarendon Press, 1976.
- [31] G. A. Bird. *Molecular Gas Dynamics and the direct Simulation of Gas Flows*, volume 42 of *Oxford Engineering Science Series*. Clarendon Press, 1994.
- [32] Yoshio Sone. *Molecular Gas Dynamics*. Birkhäuser, 2007.
- [33] G. A. Bird. *The DSMC Method*. CreateSpace Independent Publishing, 1.2 edition, 2013.
- [34] Wolfgang Wagner. A convergence proof for bird's direct simulation monte carlo method for the boltzmann equation. *Journal of Statistical Physics*, 66(3/4):1011–1044, 1992.
- [35] Michael A. Gallis, John R. Torczynski, Steven J. Plimpton, Daniel J. Rader, and Timothy Koehler. Direct simulation monte carlo: The quest for speed. *AIP Conference Proceedings*, 1628(1):27–36, 2014.

- [36] S. J. Plimpton and M. A. Gallis. SPARTA direct simulation monte carlo (DSMC) simulator. <http://sparta.sandia.gov>.
- [37] William M. Haynes, David R. Lide, and Thomas J. Bruno, editors. *CRC Handbook of Chemistry and Physics*. CRC Press, ninetyseventh edition, 2016.
- [38] Carl L. Yaws. *Handbook of Vapor Pressure*, volume Fourth. Gulf Publishing, 1995.
- [39] Ruwan Senaratne, Shankari V. Rajagopal, Zachary A. Geiger, Kurt M. Fujiwara, Vyacheslav Lebedev, and David M. Weld. Effusive atomic oven nozzle design using an aligned microcapillary array. *Review of Scientific Instruments*, 86(0232105), 2015.
- [40] Gary M. Carter and David F. Pritchard. Recirculating atomic beam oven. *Review of Scientific Instruments*, 49(120), 1978.
- [41] G. Baum, B. Granitza, S. Hesse, B. Leuer, W. Raith, K. Rott, M. Tondera, and B. Witthuhn. An optically pumped, highly polarized cesium beam for the study of spin-dependent electron scattering. *Zeitschrift für Physik D - Atoms, Molecules and Clusters*, 22:431–436, 1991.
- [42] Matthew Harvey and Andrew James Murray. Cold atom trap with zero residual magnetic field: The AC magneto-optical trap. *Physical Review Letters*, 101(173201), October 2008.

- [43] L. Bewig, U. Buck, Ch. Mehlmann, and M. Winter. Seeded supersonic alkali cluster beam source with refilling system. *Review of Scientific Instruments*, 63(3936), 1992.
- [44] R. D. Swenumson and U. Even. Continuous flow reflux oven as the source of an effusive molecular Cs beam. *Review of Scientific Instruments*, 52(559), 1981.
- [45] A. Pailloux, T. Alpettaz, and E. Lizon. Candlestick oven with a silica wick provides an intense collimated cesium atomic beam. *Review of Scientific Instruments*, 78(023102), 2007.
- [46] D. A. Reay and P. A. Kew. *Heat Pipes*. Butterworth-Heinemann, fifth edition, 2006.
- [47] Bahman Zohuri. *Heat Pipe Design and Technology*. CRC Press, 2011.
- [48] John H. Moore, Christopher C. Davis, Michael A. Coplan, and Sandra C. Greer. *Building Scientific Apparatus*. Cambridge University Press, 2009.
- [49] Stanford Research Systems, 1290-D Reamwood Ave., Sunnyvale, CA 94089. *Models RGA100, RGA200, and RGA300 Residual Gas Analyzer*, 1.8th edition, 2009.
- [50] R. Delhuille, A. Miffre, E. Lavallette, M. Büchner, C. Rizzo, G. Tréneç, J. Vigué, H. J. Loesch, and J. P. Gauyacq. Optimization of a Langmuir-Taylor detector for lithium. *Review of Scientific Instruments*, 73(2249), 2002.

- [51] Hans Pauly. *Atom, Molecule, and Cluster Beams 2: Cluster Beams, Fast and Slow Beams, Accessory Equipment and Applications*. Springer, 2000.
- [52] Thomas Rolf Mazur. *Magnetically Activated and Guided Isotope Separation*. PhD thesis, The University of Texas at Austin, August 2014.
- [53] Kirsten Viering. *Experiments to Control Atom Number and Phase-Space Density in Cold Gases*. PhD thesis, The University of Texas at Austin, August 2012.
- [54] Christopher J. Foot. *Atomic Physics*. Number 7 in Oxford Master Series in Physics. Oxford University Press, 2005.
- [55] Wolfgang Demtröder. *Laser Spectroscopy*, volume Second. Springer, fourth edition, 2008.
- [56] Wolfgang Demtröder. *Laser Spectroscopy: basic concepts and instrumentation*. Springer, 2003.
- [57] David Medellin. *Towards the creation of high-fidelity Fock states of neutral atoms*. PhD thesis, The University of Texas at Austin, August 2013.
- [58] J. Bohdansky and H. E. J. Schins. The surface tension of the alkali metals. *Journal of Inorganic and Nuclear Chemistry*, 29(9):2173–2179, September 1967.
- [59] R Calder and G. Lewin. Reduction of stainless-steel outgassing in ultra-high vacuum. *British Journal of Applied Physics*, 18(1459), 1967.

- [60] Katharina Battes, Christian Day, and Volker Hauer. Outgassing rate measurements of stainless steel and polymers using the difference method. *Journal of Vacuum Science and Technology A: Vacuum, Surfaces, and Films*, 33(021603), 2015.
- [61] Eun Ju Song. *Hydrogen Desorption in Steels*. PhD thesis, Pohang University of Science and Technology, 2015.
- [62] Y Yagodzinsky, O. Todoshchenko, S. Papula, and H. Hänninen. Hydrogen solubility and diffusion in austenitic stainless steels studied with thermal desorption spectroscopy. *Steel Research International*, 82(1):20–25, 2011.
- [63] Eun Ju Song, Dong-Woo Suh, and H. K. D. H. Bhadeshia. Theory for hydrogen desorption in ferritic steel. *Computational Materials Science*, 79:36–44, 2013.
- [64] William F. Hoshford. *Iron and Steel*. Cambridge University Press, 2012.
- [65] D. W. Jeppson, J. L. Ballif, W. W. Yuan, and B. E. Chou. Lithium literature review: Lithium’s properties and interactions. Technical Report HEDL-TME 78-15, Hanford Engineering Development Laboratory, March 1978.
- [66] Y. S. Touloukian, R. K. Kirby, R. E. Taylor, and P. D. Desai. *Thermal expansion: Metallic Elements and Alloys*. Springer Science+Business Media, 1975.

- [67] Norman F. Ramsey. *Molecular Beams*. Oxford University Press, 1956.
- [68] Dieter Meschede, editor. *Gerthsen Physik*. Springer, twentythird edition, 2006.

Vita

Lukas Gerhard Georg Gradl was born in Schweinfurt, Germany on 25 March 1994, the son of Dr. rer. nat. Gerhard Peter Eduard Gradl and Dr. med. Roswitha Katharina Gradl. Following his graduation from high school, the Kaiser Heinrich Gymnasium Bamberg, Germany, he studied Physics at the Julius Maximilians Universität Würzburg, Germany. He received his Bachelor of Science degree in Physics in August of 2015. He was accepted to the University of Texas at Austin, where he started his graduate studies in Physics in September 2015.

Permanent address: 3456 North Hills Drive, APT 333-C
Austin, Texas 78731

This thesis was typeset using GNU Emacs[†], Org-Mode[‡], and L^AT_EX[§] by the author.

[†]Emacs is the extensible, customizable, self-documenting real-time display editor of the GNU project. It is actively developed by Richard Stallman and others.

[‡]Org-Mode is a Emacs mode for keeping notes, writing TODO lists, project planning and document authoring. It was initiated in 2003 by Carsten Dominik and is maintained by Bastien Guerry at the time of writing.

[§]L^AT_EX is a document preparation system developed by Leslie Lamport as a special version of Donald Knuth's T_EX Program.